UNIVERSIDAD DE LAS AMÉRICAS PUEBLA

ESCUELA DE CIENCIAS

DEPARTAMENTO DE ACTUARÍA, FÍSICA Y MATEMÁTICAS

INFLUENCE OF ELECTRONIC CORRELATIONS ON THE STUDY OF QUANTUM CHAOS IN SIMPLE METALS

TESIS QUE, PARA COMPLETAR LOS REQUISITOS DEL PROGRAMA DE HONORES PRESENTA LA ESTUDIANTE

ZANYA GONZÁLEZ TÉLLEZ

161881

DIRECTOR: DR. MIGUEL ÁNGEL OCAÑA BRIBIESCA

SAN ANDRÉS CHOLULA, PUEBLA. OTOÑO, 2023

TESIS QUE, PARA COMPLETAR LOS REQUISITOS DEL PROGRAMA DE HONORES PRESENTA LA ESTUDIANTE ZANYA GONZÁLEZ TÉLLEZ
161881

DIRECTOR DE TESIS

Dr. Miguel Ángel Ocaña Bribiesca

PRESIDENTE DE TESIS

Dra. Milagros Zeballos Rebaza

SECRETARIO DE TESIS

Dr. Juan Francisco Rivas Silva

Contents

Abstract

In this thesis, we conduct a thorough analysis of the statistical properties associated with the band structures of Silicon and Cerium. Our research shows that Density Functional Theory (DFT) calculations can indeed exhibit quantum chaos, aligning with the predictions of Random Matrix Theory. Furthermore, our investigation explores the influence of the Hubbard correction on the Cerium band structure, a correction essential for precise descriptions of strongly correlated systems. We study the relationship between the manifestation of chaotic behavior and the use of varying values for this correction. We find that our results for Silicon closely mirror the discoveries of Mucciolo and collaborators. Additionally, we successfully diagnose chaotic behavior in certain Cerium calculations.

Palabras clave: Silicon, Cerium, Random Matrix Theory, Level Spacing, Velocity.

1 Introduction

The study of classical systems that exhibit what is known as chaotic behavior has been a subject of extensive exploration for many years (Taylor & Taylor, 2005). It has reached a point where different methods have been developed to obtain an acceptable description and understanding of systems highly sensitive to changes in initial conditions and that do not display periodic behavior. Nonetheless, with the development of quantum mechanics, a question has arisen: can quantum systems also exhibit chaos, and can we explain quantum chaotic behavior using similar tools as those commonly employed to diagnose classical chaos? This question has been widely addressed and studied for different quantum systems and remains relevant today (Luna-Acosta, Na, Reichl, & Krokhin, 1996; M. V. Berry, 2001; Escalante & Skipetrov, 2018).

It is widely recognized that to gain a comprehensive understanding of a quantum system, we need to know its Hamiltonian, which contains all the interactions necessary for describing the system. Subsequently, we must solve the Schrödinger equation to obtain the physical properties of interest. However, when it comes to the study of certain quantum systems, numerous challenges arise when attempting to derive the Hamiltonian and subsequently solve the Schrödinger equation (Mehta, 1967). This has prompted the search for alternative methods to analyze the physical properties of quantum systems.

During the early 1950s, Eugene Wigner studied the statistical properties of nuclear spectra (Wigner, 1967). From his work, Wigner discovered that the distribution of spacings between energy levels in the Uranium nucleus could be accurately described by the distribution of eigenvalues of Hermitian matrices with entries composed of random numbers. This revelation also implied that the energy spectra exhibited what today is known as quantum chaos, an observation made by McDonald and Kaufman from their studies on a free particle with stadium boundaries whose classical counterpart is chaotic (McDonald & Kaufman, 1979). Wigner's breakthrough set the stage for the exploration of other chaotic quantum systems, such as quantum billiards, whose energy spectrum statistics exhibited clear connections with the predictions of Random Matrix Theory.

In 1994, Mucciolo, Capaz, Altshuler, and Joannopoulos published the paper 'Manifestation of quantum chaos in electronic band structures' (Mucciolo, Capaz, Altshuler, & Joannopoulos, 1994). In this work, they investigated the prospect of encountering chaos in the energy spectra of periodic structures, like crystals. Their study revealed that chaotic behavior could be identified in specific regions of the Silicon band structure and explored the transition to chaos in the supercrystal $Al_xGa_{1-x}As$ alloy band structure. Inspired by their findings, this thesis centers on the statistical analysis of the energy spectrum of strongly correlated electronic systems; such as Cerium, with a focus

on discovering chaotic behavior in particular segments of its band structure.

The primary objective of this work is to utilize Density Functional Theory (DFT) via the software WIEN2K to obtain the band structures of Silicon and Cerium and compute their level spacing distributions to explore the potential presence of chaotic behavior, as predicted by Random Matrix Theory. This thesis places a specific focus on the study of the level spacing distribution of Cerium when the Hubbard correction is applied. The Hubbard correction consists of employing an empirical parameter required to accurately describe the electronic interaction in strongly correlated systems. The goal is to investigate whether the use of this correction leads to chaotic behavior in particular regions of Cerium's band structure.

Our approach begins with the study of the band structure of Silicon. The relevance of doing this is to verify the possibility of finding regions in the spectrum where the bands exhibit chaotic behavior. Additionally, we seek to confirm that quantum chaos can be detected in structures computed using DFT methods, in comparison with the original pseudopotential approximation employed by Mucciolo and collaborators.

Subsequently, we transition to the analysis of Cerium. It has been observed that DFT may present deficiencies when modeling elements with partially filled d and f orbitals. These shell electrons are localized, demanding precise descriptions of the interactions between them. Cerium, along with metals known as lanthanides and actinides, falls into this category, with valence electrons in the d and f shells. To accurately model these metals, we must introduce electron correlations through a parameter or potential. A preliminary approach to make this correction is through the LDA+U method, which involves employing a parameter known as Hubbard U. The Hubbard U parameter accounts for Coulomb and exchange interactions between orbitals. Through this approach, we aim to analyze the changes in Cerium's structure when different values of the U parameter are employed and determine if the statistical analysis we will perform can help us identify the most appropriate U value for describing this metal. We want to focus primarily on the study of the energy spectrum when the U parameter is set between 6 eV and 7 eV, the range recommended by Anisimov and other authors for Cerium (V. Anisimov & Gunnarsson, 1991).

This approach is relevant because, although pure Cerium may not be of significant interest today, it finds applications in various areas and possesses intriguing properties when used as a dopant in semiconductors like ZnO (Zhang, Zhang, & Xu Wang, 2011). It is also widely studied when combined with oxygen to form Cerium oxides (Bennett & Jones, 2014; Schafer, Daelman, & Lopez, 2021). All these systems necessitate the application of the Hubbard correction for precise descriptions. Therefore, it is essential to explore new methods for determining the most accurate value of U for each system.

This work investigates whether the diagnosis of quantum chaos could serve as a valuable tool for determining the Hubbard U parameter.

This thesis is organized as follows. We commence in Chapter 2 with a general introduction to chaotic behavior in classical and quantum systems. Within this section, we also look into Mucciolo's work in identifying chaotic behavior in crystalline structures, serving as the primary reference for this thesis. Subsection 2.1 is completely dedicated to introducing Random Matrix Theory as a valuable tool for studying chaotic behavior in quantum systems. In this subsection, we revisit Wigner's original work on the connection between nuclear-level spacing distributions and Random Matrix Theory. Additionally, we introduce the Gaussian ensembles proposed by Dyson, which will serve to diagnose quantum chaos in this thesis. Following the introduction of RMT, in subsection 2.2 we broadly present how the statistics of random matrices became a tool to diagnose chaos in quantum systems.

Subsection 2.3 focuses on presenting fundamental concepts related to Density Functional Theory, the method employed to derive the band structures of Silicon and Cerium. Within this subsection, we also introduce the Hubbard correction, an important component for accurately describing systems where electrons present strong correlations between each other, such as Cerium. The U parameter from the Hubbard correction plays an important role in our investigation of the behavior of the Cerium structure.

In Chapter 3, we present the results obtained and their analysis. Subsections 3.1 and 3.2 provide insights into the optimized parameters and approximations used to obtain the structures of Silicon and Cerium, both derived through the WIEN2K software for solid-state calculations. We also offer detailed descriptions of the conventional cell, Brillouin zone, and band structure for both Silicon and Cerium. In the case of Cerium, we also include a comprehensive overview of the Density of States for the structure, both with and without the Hubbard correction, as well as for various calculations with different values of the U parameter. This exploration aims to understand how the contributions of the d and f orbitals to the structure change when the Hubbard correction is applied, imperative to correctly justify the statistical analysis conducted.

Subsection 3.3 is dedicated to the analysis of the level spacing distributions for Silicon and Cerium. In the case of Silicon, our goal is to replicate Mucciolo's findings and show that chaotic behavior can be found in the band structure of simple metals when utilizing DFT to obtain them. For Cerium, we conduct an in-depth analysis of the level spacing distribution for a select set of bands in different Ce calculations, both with and without the Hubbard correction. This investigation is aimed at understanding the impact of considering the correlation-exchange interaction between electrons in the band structure. Subsequently, in Subsection 3.4, we shift our focus to the analysis of velocity

distributions for the band structures of Silicon and Cerium, once more with a particular emphasis on the examination of Cerium's distributions when the Hubbard correction is applied.

Finally, Chapter 4 is dedicated to the concluding remarks of the thesis. Within this chapter, we recap the most significant findings and their possible implications. Furthermore, we delve into the questions and additional challenges that have emerged from this work and explore potential subjects for future research.

2 Theoretical Background

In classical mechanics, it has been observed that multiple systems described by nonlinear equations exhibit chaotic behavior. Chaotic systems possess distinct characteristics, the most prominent being their sensitivity to initial conditions and lack of periodicity. The sensitivity to initial conditions implies that even a slight variation in the initial state of a system leads to entirely different trajectories (Taylor & Taylor, 2005). Since it is practically impossible to precisely know the initial conditions of a system, our approximations of this state often involve specific errors and, as a result, describing a chaotic system becomes a challenging task. Furthermore, the non-periodic nature of chaotic systems indicates that their long-term motion is erratic and does not converge to any specific pattern, making it difficult for us to predict their future behavior (Strogatz, 2018). In nature, numerous systems demonstrate chaos, and this is precisely why the study of such systems holds immense significance.

After reviewing chaotic behavior in classical systems, one might be tempted to search for similar chaos in their quantum analogs. However, such efforts prove to be futile as it has been observed that the chaotic behavior of classical processes is mitigated when approached from a quantum perspective (Gutzwiller, 2013). Nonetheless, interesting properties have been discovered in certain quantum systems as their classical counterparts suffer a transition to chaos, especially when studying the statistical aspects of energy spectra (Reichl, 2004). To resolve the quantum chaos contradiction, Berry (M. Berry, 1989) proposed the term ”quantum chaology” to define the study of semiclassical systems, where Planck's constant tends to zero, and whose classical analogs exhibit chaotic behavior.

The study of chaos in quantum systems experienced a revolutionary transformation upon the discovery of a profound connection between random matrix theory and the statistics of quantized chaotic systems, such as quantum billiards (Reichl, 2004). As we shall observe in the next subsection, random matrix theory finds significant application in explaining the statistical distribution of nuclear energy levels, which leads us to infer that energy spectra could display chaotic behavior. Quantum chaos is now even searched for in crystals. In his paper, Mucciolo studies the statistical properties of different crystal band structures in an attempt to find a behavior that should be true for any crystalline structure (Mucciolo et al., 1994).

Finally, another fundamental characteristic that needs to be taken into account when searching for quantum chaos is the symmetry of the system. It is well known that the energy spectrum of nuclei, atoms, and other quantum systems tends to have degeneracies that are more likely to appear if there are symmetries. These degeneracies are also con-

nected with the chaoticity of the classical system since it has been observed that when there exist symmetries in systems they don't exhibit chaotic behavior (Reichl, 2004). In crystalline structures, symmetries can be broken by avoiding symmetry points in the Brillouin zone while analyzing the band structure.

2.1 Random Matrix Theory

Random Matrix Theory (RMT) is a branch of mathematics that has captured the attention of various physicists due to its numerous applications, which have proven to be useful in comprehending complex systems. One of the challenges that significantly contributed to the advancement of random matrix theory in physics was the description of the heavy U^{239} nucleus (Mehta, 1967). It is well known that nuclei have discrete energy levels, similar to those where electrons can be found, which arise when the Schrödinger equation is solved (Krane, 2019). The lowest excited states can be clearly studied using different approximations of the potential energy of the nucleus given that it is not possible to express this quantity simply. However, difficulties emerge when we try to describe higher excited states since the approximations to the potential become inaccurate, then, it is convenient to use an average of the energy level properties.

The energy and the functions that describe the particles that form the nucleus can be obtained through the solution of the Schrödinger eigenvalue problem $H\Psi_i = E_i\Psi_i$. To solve this equation, we first need to define the Hamiltonian operator H, which is a matrix that commonly contains the kinetic and potential interactions of the particles in the system being analyzed. Nevertheless, we previously stated that obtaining the potential of the nucleus is a complicated task, then it is convenient to make statistical approximations. Classically, it was thought that we could use an average ensemble of different Hamiltonians that could describe different nuclei, and then use this ensemble to describe any other particular nucleus. This assumption seemed convincing until it was observed that it is not possible to correctly describe the U^{239} nucleus using this approach (Mehta, 1967).

Wigner solved this problem when he proposed to treat the Hamiltonian as a symmetric matrix whose elements should be random variables (Mehta, 1967). He suggested this when he noticed certain resemblances between the statistical characteristics of energy levels and the eigenvalues of a random matrix. According to Wigner (Wigner, 1967), the level spacing distributions must obey the following rules:

1. When energy levels have the same spin and parity, their spacing distribution should

be given by the function:

$$p(x) = \frac{\pi}{2} x e^{-\frac{\pi}{4}x^2} \qquad x = \frac{S}{D} \tag{1}$$

where *S* is a given distance between levels and *D* is the mean spacing.

2. The energy levels with different spin or parity do not correlate. Therefore it is possible to approach this sequence by creating a random superposition of simple sequences, which are the ones with the same spin and parity.

In Figure 1 we can observe the distribution defined by Wigner's first rule, as well as the plot resulting from randomly superimposing two systems of levels with equal mean spacing. The third curve in the graph is the exponential which describes a Poisson-like distribution, which represents the level spacing distribution one would obtain if levels were completely random.

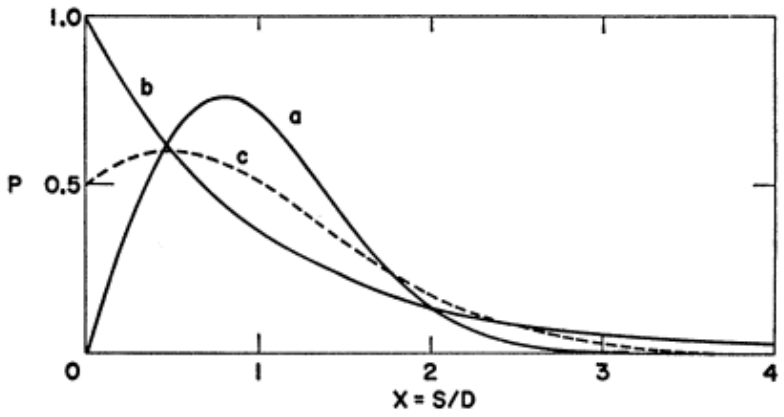

Figure 1: Plot of Wigner's distributions (Rosenzweig & Porter, 1960). (a) is the distribution proposed by Wigner and presented in eq.(1), (b) represents the Poisson distribution, and (c) is the superposition of levels that model levels with different spin and parity.

The distribution of spacing between energy levels, in particular, collected significant interest and was extensively examined by Rosenzweig and Porter (Rosenzweig & Porter, 1960). In their research, they discovered that the likelihood of energy levels being extremely close to one another was practically zero, thereby validating Wigner's postulate. Subsequently, Dyson (Dyson, 1962) studied RMT through a group-theory approach and proposed to divide random matrix ensembles, invariant under the Gaussian symmetry group, into three different classes: Gaussian orthogonal (GOE), Gaussian unitary (GUE)

and Gaussian symplectic (GSE). Each of these ensembles will be discussed in the following subsection.

Gaussian Ensembles

The way the spacing between levels is distributed can be approximated to some extent using the distribution Wigner proposed. Nevertheless, depending on the circumstances and characteristics of the system, we may need to use different ensembles to describe the level spacing distribution. As we already know, the atomic nucleus and other quantum systems can be described through the Hamiltonian operator, which is a Hermitian matrix. Furthermore, its entries are supposed to be random to assure statistical independence between variables and which symmetry conditions can vary according to the following ensembles.

Gaussian Orthogonal Ensemble

The Gaussian Orthogonal Ensemble (GOE) is a slightly more formal variation of the Gaussian ensemble proposed by Wigner and is used to describe even-spin systems, which are invariant under time-reversal transformations, represented by symmetric matrices (Mehta, 1967). In one of his papers, Dyson (Dyson, 1962) defines the GOE as follows:

Definition 2.1. The Gaussian Orthogonal Ensemble is uniquely defined as the one that contains all symmetric unitary matrices *S* and fulfills the following condition:

- The matrices that compose the ensemble are invariant under the transformation

$$S \to W^T S W \tag{2}$$

of the space of real symmetric matrices into itself, where *W* is any unitary matrix.

In other words, Dyson stated that the probability $P(dS)$ of finding a system in this ensemble that belongs to the volume element dS is invariant under the transformation in eq.(2). This in turn means that the GOE is an ensemble in the space of symmetric unitary matrices, which contains all the matrices *S* with equal probability of occurrence. The probability distribution function of the Gaussian orthogonal ensemble is:

$$P_{GOE}(t) = \frac{\pi}{2} t e^{-\frac{\pi t^2}{4}} \tag{3}$$

Gaussian Unitary Ensemble

The Gaussian Unitary Ensemble (GUE) is the most simple ensemble of the three reviewed in this work. It can be applied to describe systems that are not invariant under time-reversal transformations, which means that they can be associated with Hermitian matrices that are not necessarily symmetric or self-adjoint. The formal definition of this ensemble as stated by Dyson is:

Definition 2.2. The Gaussian Unitary Ensemble is uniquely defined in the space of unitary matrices. The matrices *S* that compose the ensemble must satisfy the condition of being invariant under the transformation

$$S \to USW \tag{4}$$

of the space of unitary matrices into itself, and where *U*, *W* are any two unitary matrices.

This ensemble could be used to study different quantum systems under external electric fields, which need to be strong enough to significantly alter the unperturbed level structure. Therefore, we could only use this ensemble while analyzing atomic or molecular systems (Dyson, 1962). The probability distribution function of the Gaussian unitary ensemble is:

$$P_{GUE}(t) = \frac{32}{\pi^2} t^2 e^{-\frac{4t^2}{\pi}} \tag{5}$$

Gaussian Symplectic Ensemble

For our purposes, it is sufficient to understand the Gaussian orthogonal and the unitary ensembles, however, we will briefly review the symplectic ensemble for completeness. In contrast with the orthogonal ensemble, the Gaussian Symplectic Ensemble (GSE) is primarily used to describe odd-spin systems, which are invariant under time-reversal transformations but cannot be represented through symmetric matrices. To overcome the difficulties generated due to the non-symmetric nature of these systems, Dyson (Dyson, 1962) cleverly used the advantages of quaternion algebra[1] to simplify the manipulation of matrices. According to Dyson, the symplectic ensemble can be defined as follows:

Definition 2.3. The Gaussian Symplectic Ensemble is uniquely defined in the space of self-dual unitary quaternion matrices. The matrices *S* that compose the ensemble must

[1]Quaternion algebra is an algebra in the field of real numbers *R*, of dimension 4. A general element of this algebra has the form $\sum_{i=0}^{3} a_i e_i$, where a_i are real coefficients and e_i are elements of the algebra (Chevalley, 1947).

satisfy the property of being invariant under the transformation

$$S \rightarrow W^R S W \tag{6}$$

where W is a unitary matrix and W^R is the time reversal operation applied to W. The matrix W is called self-dual when $W = W^R$.

2.2 Quantum Chaos

Wigner and other authors who previously explored the statistical properties of nuclear spectra established the relationship between random matrix theory and the statistical distribution of nuclear energy levels. However, they did not delve into the potential implications of chaotic behavior in quantum systems whose statistical properties are described by RMT.

The pivotal connection between Random Matrix Theory and quantum chaos was made by McDonald and Kaufman in 1979 when they studied quantum systems characterized by Hamiltonians displaying stochastic trajectories (McDonald & Kaufman, 1979). This breakthrough evoked increased interest in exploring quantum systems by numerous researchers. Notably, extensive work focused on investigating the statistical properties of two-dimensional quantum billiards. Their study revealed that integrable billiards adhere to Poisson distribution statistics. In contrast, the spectrum of nonintegrable quantum billiards, arising from classically chaotic systems, displays a significant reduction in level spacing values near zero and exhibits closer alignment with predictions from RMT (Reichl, 2004).

Following this connection, it became common to use RMT as a tool to diagnose quantum chaos in a system. The energy spectra of other systems, such as atoms and molecules, began to be studied in the quest for stochastic behavior. Of particular interest is the work of Mucciolo and collaborators, who aimed to demonstrate that quantum chaotic behavior should be observable in the energy spectra of crystalline structures when varying the block momenta $\vec{k}$ of the periodic Hamiltonian to identify spaces where symmetries are broken.

2.3 Density Functional Theory

One of physics's main interests is understanding matter's properties from an atomic perspective. It is well known that the Schrödinger equation models the behavior of atoms and molecules, and through it, we can obtain the energy of the system being analyzed

(Szabo & Ostlund, 2012). The time-independent Schrödinger equation that describes a system with *N* electrons of mass *m* is presented in eq.(7).

$$\left[\frac{h^2}{2m}\sum_{i=1}^{N}\nabla_i^2+\sum_{i=1}^{N}V(\mathbf{r}_i)+\sum_{i=1}^{N}\sum_{j<i}U(\mathbf{r}_i,\mathbf{r}_j)\right]\Psi=E\Psi \tag{7}$$

In this equation, the Hamiltonian operator is composed of the terms in brackets, which are respectively the kinetic energy of each electron, the interaction between each electron and the nucleus, and the interaction between electrons. The valuable information in this equation comes from the eigenfunction Ψ, referred to as the wave function. This function depends on the coordinates of each electron and encapsulates information about the system under examination. Additionally, the eigenvalue *E* holds significance as it represents the total energy of the system.

In a precise analysis, comprehending the complete behavior of our system demands the inclusion of both the kinetic energy of the nuclei and their mutual interactions. Nevertheless, in the Schrödinger equation presented, we have already adopted the Born-Oppenheimer approximation (Szabo & Ostlund, 2012). This approximation is based on the recognition that the movement of nuclei occurs at a considerably slower pace compared to the movement of electrons. As a result, when attempting to solve exclusively the electronic problem, we are justified in neglecting the nuclear terms.

Furthermore, when characterizing many-electron systems, it is sometimes convenient to write the electronic wave function in terms of the spatial orbitals $\psi_i(\mathbf{r})$, which are wave functions for individual electrons (Szabo & Ostlund, 2012). To achieve this, Slater determinants come into play. They allow us to represent the entire wave function in terms of the single electrons within the system, while simultaneously adhering to the Schrödinger equation and the Pauli exclusion principle, which states that the wave function of the system must be antisymmetric (Szabo & Ostlund, 2012).

The Slater determinant for an N-electron system is defined in equation (8), where $(\mathbf{r}_1,\mathbf{r}_2,...,\mathbf{r}_N)$ denote the electrons of the system, and $(\psi_i,\psi_j,...,\psi_k)$ represent the spatial orbitals they can inhabit.

$$\Psi=\frac{1}{\sqrt{N!}}\begin{vmatrix}\psi_i(\mathbf{r}_1) & \psi_j(\mathbf{r}_1) & ... & \psi_k(\mathbf{r}_1)\\ \psi_i(\mathbf{r}_2) & \psi_j(\mathbf{r}_2) & ... & \psi_k(\mathbf{r}_2)\\ : & : & : & :\\ \psi_i(\mathbf{r}_N) & \psi_j(\mathbf{r}_N) & ... & \psi_k(\mathbf{r}_N)\end{vmatrix}$$

As previously stated, the wave function contains the spatial information of every electron. Nevertheless, it is sometimes more useful to express this information in terms of the probability density. The probability of finding electron *i* at a point ***r*** in the volume element ***dr*** is given by eq.(8).

$$P(\mathbf{r})d\mathbf{r} = |\psi_i|^2 d\mathbf{r} \tag{8}$$

Then, we can define the probability of finding any electron in volume ***dr*** at ***r*** as follows:

$$n(\mathbf{r})d\mathbf{r} = 2\sum_{i}^{N/2} |\psi_i|^2 d\mathbf{r} \tag{9}$$

The term ***n(r)*** is the density of electrons at point ***r*** and the factor of 2 at the beginning of eq.(9) accounts for the two electrons with a different spin that each spatial orbital contains (Szabo & Ostlund, 2012). The integral over the whole space of the electron density will yield the total number of electrons.

For the Hydrogen atom, obtaining the exact wave function and energy is possible because there is no interaction between electrons, which makes the Schrödinger equation significantly simpler and lets us treat it as a simple eigenvalue problem. However, to solve the equation for atoms with multiple electrons, it is necessary to consider the electron-electron interaction, which makes the Schrödinger equation a complicated many-body problem. Furthermore, we need to know the spatial orbital of each electron to construct the wave function, as suggested by eq.(8), this increases exponentially the dimension of the problem (Sholl & Steckel, 2022).

To solve the Schrödinger equation for problems that involve more than 3 electrons, it is common to use approximation methods. The majority of these approximation techniques are rooted in the variational method, devised to provide the best feasible solutions guided by the variational principle. To comprehend this principle, it is pertinent to revise the Schrödinger equation. The system's energy can be expressed as the expectation value of the Hamiltonian operator,

$$< \Psi|\hat{H}|\Psi >= E < \Psi|\Psi > \tag{10}$$

where the eigenfunction of the problem is represented using Dirac notation. The variational principle states that when provided with an approximate wave function Ψ', the corresponding expectation value of the Hamiltonian becomes:

$$< \Psi' | \hat{H} | \Psi' > \geq E_0 \tag{11}$$

signifying that the employment of the approximate wave function yields an energy value that is an upper bound for the ground state energy (Szabo & Ostlund, 2012). Consequently, it can be inferred that if the precise wave function of the system were known, the determination of the system's ground state energy E_0 would be feasible. This highlights that the primary objective of approximation methods is to approach the ground state energy of the system as closely as possible.

Hohenberg-Khon Theorems

Many of the various approximation methods used today to study systems with multiple electrons are based on the fundamental ideas of density functional theory (DFT), which originated from the proofs of Hohenberg and Khon's theorems (Hohenberg & Kohn, 1964). The first theorem states:

Theorem 1 (Hohenberg-Kohn 1)**.** *For a system under the influence of an external potential $\nu(\boldsymbol{r})$, the potential $\nu(\boldsymbol{r})$ is a unique functional of the electron density n(**r**); and, in turn, the full many-particle ground state is a unique functional of n(**r**).*

This theorem establishes that it is possible to determine a unique external potential $\nu(\mathbf{r})$ through the electron density. From this result, it follows that using the complete Hamiltonian which contains the external potential previously obtained, we can find the exact energy and wave function of the system (Martin, 2020). The second Hohenberg-Khon theorem affirms:

Theorem 2 (Hohenberg-Kohn 2)**.** *It is possible to define the energy functional $E[n]$ for a given potential $\nu(\boldsymbol{r})$. The electron density for which $E[n]$ assumes its minimum value is the exact ground state electron density $n_0(\boldsymbol{r})$ that solves the Schrödinger equation.*

To prove this theorem, Hohenberg and Kohn define the energy functional for a certain potential as:

$$E[n] = F[n] + \int \nu(\mathbf{r}) n(\mathbf{r}) d\mathbf{r} \tag{12}$$

where $F[n]$ is the functional that contains the kinetic and interaction energies valid for any system involving interacting electrons and therefore referred to as universal (Hohenberg & Kohn, 1964).

Together, the theorems indicate that electron density alone determines all the unique properties of the system being analyzed. Furthermore, if the complete energy functional $E[n]$ was known, it would be sufficient to find the electron density which minimizes the value of the functional to calculate the exact ground state energy and wave function. Nevertheless, it is important to notice that the Hohenberg-Khon theorems provide no insight into how we can determine the exact form of the functional (Sholl & Steckel, 2022).

Khon-Sham Equations

The Hohenberg-Khon approach to solving the many-body problem involved dealing with a functional which must contain the interactions between multiple electrons, making it difficult to find the exact form of this functional. In 1965, Kohn and Sham proposed replacing the original problem with a system of non-interacting particles, that could be represented through single electron equations (Kohn & Sham, 1965). According to Hohenberg and Kohn, we can take out from the functional $F[n]$ the contribution from the Coulomb interaction between electrons and write the ground state energy of the system as follows:

$$E[n] = \int \nu(\mathbf{r})n(\mathbf{r})d\mathbf{r} + \frac{e^2}{2}\int\int \frac{n(\mathbf{r})n(\mathbf{r'})}{|\mathbf{r}-\mathbf{r'}|}d\mathbf{r}d\mathbf{r'} + G[n] \tag{13}$$

Khon and Sham proposed that the new functional $G[n]$, presented in eq.(14), should contain the kinetic energy of the non-interacting electrons and all the exchange and correlation effects of the interacting system, which are included through the exchange-correlation functional $E_{XC}[n]$.

$$G[n] = T_s[n] + E_{XC}[n] \tag{14}$$

Then, it is possible to solve a set of single-electron equations and obtain the ground state density of the whole interacting system, where the accuracy of our result will depend only on which approximation to the exchange-correlation functional we choose (Martin, 2020). In eq.(15), we present the Kohn-Sham single-electron equations.

$$\left[\frac{h^2}{2m}\nabla^2 + V(\mathbf{r}) + V_H(\mathbf{r}) + V_{XC}(\mathbf{r})\right]\psi_i = \epsilon_i\psi_i \tag{15}$$

In these equations, the terms inside the bracket are respectively the kinetic energy of a single electron and all the potentials needed to describe the interactions between an electron and the other particles of the system. The first potential $V(\mathbf{r})$ represents

the Coulomb interaction between the electron being analyzed and all the nuclei of the system. The second potential term is known as the Hartree potential, which describes the interaction between the i-th electron and the density $n(\mathbf{r}')$ due to the remaining electrons (Sholl & Steckel, 2022). The Hartree potential can be written as:

$$V_H(\mathbf{r}) = e^2 \int \frac{n(\mathbf{r}')}{|\mathbf{r} - \mathbf{r}'|} d\mathbf{r} \tag{16}$$

The third and last potential is the exchange-correlation potential $V_{XC}(\mathbf{r})$, which comprises all the remaining interactions between particles and can be written in terms of the energy functional $E_{XC}[n]$ as follows:

$$V_{XC}(\mathbf{r}) = \frac{\partial E_{XC}}{\partial \mathbf{r}} \tag{17}$$

We observe that to solve the Kohn-Sham equations and obtain the electron density, which depends on the single electron wave functions, we first need to know the Hartree potential. However, to calculate the Hartree potential we need to know the electron density, which makes this problem a self-consistent one that can be solved through iterations.

Exchange-Correlation Functional

The main concern in DFT is finding the appropriate exchange-correlation functional (Martin, 2020). Kohn and Sham showed that for a uniform electron gas of density n, it is sufficient to approximate the energy functional as the exchange-correlation energy per electron at a certain point in space $\mathbf{r}$, as presented in eq.(18). In other words, we can approximate the energy functional E_{XC} using the local density.

$$E_{XC}[n] = \int n(\mathbf{r}) \epsilon_{XC}^{unif}(n(\mathbf{r})) d\mathbf{r} \tag{18}$$

The approach developed by Kohn and Sham is known as the local density approximation (LDA), which proves highly effective in solving the Kohn-Sham equations with acceptable accuracy. Nevertheless, it is important to acknowledge that the local density approximation is not the sole method for estimating the exchange-correlation functional. With the introduction of Density Functional Theory (DFT), various functional proposals have surfaced, and among them, the widely known generalized-gradient approximations, hold particular significance for the objectives of this study.

Generalized-Gradient Approximations

Generalized-Gradient Approximations (GGAs) have emerged as a means of enhancing the existing LDA. They take into account not only the local density information of the

system but also incorporate the gradient of the density. This allows for the consideration of spatial information when dealing with systems lacking uniform density (Sholl & Steckel, 2022). The energy functional using this approximation is defined as follows:

$$E_{XC}^{GGA}[n] = \int n(\mathbf{r})\epsilon_{XC}(n, |\nabla n|)d\mathbf{r} \tag{19}$$

where ∇n is the gradient of the density. Since GGAs were created to improve the local density approach, it is convenient to express eq.(19) in a way that is related to the LDA functional so that it is possible to recover the uniform electron gas approximation at a certain limit. Therefore, we write:

$$E_{XC}^{GGA}[n] = \int n(\mathbf{r})\epsilon_{X}^{unif}(n)F_{XC}(n, \nabla n)d\mathbf{r} \tag{20}$$

In this equation, F_{XC} represents the enhancement factor, enclosing all gradient effects, whereas ϵ_X^{unif} corresponds to the exchange energy per electron for the uniform electron gas. There are numerous ways to parameterize F_{XC}. Among the most widely used, and the one employed in the calculations presented here, is the parametrization proposed by Perdew, Burke, and Ernzerhof (GGA-PBE) (Perdew, Burke, & Ernzerhof, 1996). In their work, they defined distinct exchange and correlation functionals, each possessing a distinct enhancement factor. These factors are constructed solely using fundamental constants, allowing for the retrieval of the local approximation. The expression for the exchange enhancement factor is:

$$F_X(s) = 1 + \kappa - \frac{\kappa}{1 + \mu s^2/\kappa} \tag{21}$$

where $\kappa = 0.804$ and $\mu = 0.21951$. On the other hand, the gradient contribution in the energy correlation functional is taken into account through the following ansatz:

$$H = \frac{e^2}{a_0}\gamma\phi^3 ln\left[1 + \frac{\beta}{\gamma}t^2\left(\frac{1 + At^2}{1 + At^2 + A^2t^4}\right)\right] \tag{22}$$

where γ and β are constants, e is the electron charge, a_0 the Bohr radius and A is defined as follows:

$$A = \frac{\beta}{\gamma}\left[exp\left(-\frac{\epsilon_C^{unif}}{\gamma\phi^3 e^2/a_0}\right) - 1\right]^{-1} \tag{23}$$

Hubbard's U Parameter

The exchange-correlation functionals presented previously have been widely used to describe many electronic systems with great accuracy. Nevertheless, in systems where electrons have a strong interaction, like materials with partially filled d and f orbitals, the LDA and the GGA cannot correctly describe the correlation between electrons. There are multiple ways to face this issue and improve the exchange-correlation functional. We are especially interested in the LDA+U approach, which uses the already-known local density calculations with the necessary orbital interactions by adding a parameter known as Hubbard's parameter U, proposed by Anisimov and his collaborators (V. I. Anisimov, Aryasetiawan, & Lichtenstein, 1997).

The LDA+U method separates the electrons that constitute the systems into two categories: the ones located on the d or f orbitals and those in the inner s and p orbitals. The electron located in the inner orbitals can be described using only the local density or generalized-gradient approximation. On the other hand, the outer electrons are most of the time localized electrons, which means they lay in a specific region between atoms. Since the LDA method treats the interaction between electrons as an average, it is necessary to include a term that takes into account the Coulomb interaction between outer electrons. Therefore, the new functional that involves the missing interaction is:

$$E^{LDA+U} = E^{LDA}[n] + \frac{U-J}{2}\sum_{l,j,\sigma}\rho^{\sigma}_{lj}\rho^{\sigma}_{jl} \tag{24}$$

The last term is the Hubbard modification. Here, U is the Hubbard parameter, which represents the Coulomb interaction between electrons, and J is the exchange term associated with the orbitals of interest. The term ρ^{σ}_{jl} is the density matrix of the electrons that occupy the outer orbitals and σ the spin index (Dudarev et al., 2000).

2.4 Determination of Electronic Structure

To solve the Kohn-Sham equations, various methods are available. We will employ diverse approaches to determine different electronic structures depending on the system under examination. When dealing with crystals, we first need to understand that due to the periodic arrangement of the atoms in them, we can reduce the study of the electrons to one unit cell, since the effect of an operator like the Hamiltonian should be invariant under lattice translations (Martin, 2020). Then, the Schrödinger equation reduces to the following:

$$\left[-\frac{\hbar^2}{2m}(\nabla + i\mathbf{k})^2 + V(\mathbf{r})\right] u_{\mathbf{k}}(\mathbf{r}) = E_{\mathbf{k}} u_{\mathbf{k}}(\mathbf{r}) \tag{25}$$

where the term in brackets is the Hamiltonian operator, **k** is a vector in the reciprocal space and $u_{\mathbf{k}}$ is the periodic wavefunction.

Following this approach for a periodic structure, it has been observed that the most accurate solutions for the Kohn-Sham equations are achieved through the linearized augmented plane wave method (LAPW) (Blaha et al., 2001). This method aims to linearize and thus simplify the equations derived from Slater's augmented plane wave method (APW).

Augmented plane waves are techniques that belong to the family of atomic sphere methods. These methods involve the partitioning of the electronic structure of the system into distinct regions: the vicinity surrounding the atoms and the interstitial spaces between them. By employing distinct basis sets following the spatial area of interest, we only need to match the functions in the boundaries to solve the problem. In the LAPW method, if we are studying a solid, the unit cell is divided into two main regions as presented in Fig. 2.

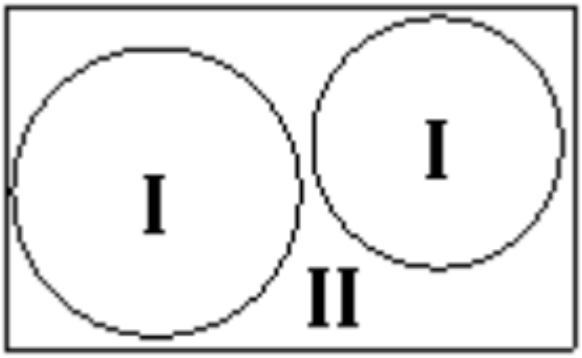

Figure 2: Division of the unit cell (Blaha et al., 2001).

In the spherical area surrounding the atoms (I), the potential assumes the form of the actual atomic potential. Here, the basis set is constructed through a linear combination of atomic-like functions. These functions consist of radial components combined with spherical harmonics. The specific basis functions employed by the LAPW method for the region are:

$$\chi^{LAPW}_{\mathbf{k}+\mathbf{G}_m} = \sum_{lm} [A_{lm}(\mathbf{k}+\mathbf{G}_m)\psi_l(r, E_l) + B_{lm}(\mathbf{k}+\mathbf{G}_m)\dot{\psi}_l(r, E_l)] Y_{lm}(\mathbf{r}) \tag{26}$$

To linearize the traditional APW method, we need to use a linear combination between the radial solution of the Schrödinger equation ψ_l and its derivative $\dot{\psi}_l$, as presented in eq.(26). In this equation, E_l is the energy of the localized sphere, **k** is the wave vector in the Brillouin zone and $\mathbf{G}_m$ are the reciprocal lattice vectors. The coefficients A_{lm} and B_{lm} are functions of $\mathbf{k} + \mathbf{G}_m$. On the other hand, in the interstitial region (II) we want to use a more general function to construct the basis set since the potential is smooth and almost constant in this region. Therefore, the LAPW method uses plane waves as basis functions for region II, which are presented in the following expression:

$$\chi^{LAPW}_{\mathbf{k}+\mathbf{G}_m} = exp(i(\mathbf{k} + \mathbf{G}_m) \cdot \mathbf{r}) \tag{27}$$

Then, we can write the Kohn-Sham equations on the basis proposed and solve them to find the desired information about the system.

3 Results and Discussion

The band structure of Silicon and Cerium was obtained using the WIEN2K program, which employs the linearized augmented plane wave (LAPW) method. The initial structure of Silicon was constructed with a lattice constant of $a = 5.430$ Å, belonging to the $227\_Fd\text{-}3m\_$ space group. On the other hand, the initial structure of Cerium was constructed using the lattice parameters $a = 3.649$ Å, $b = 3.649$ Å, and $c = 5.959$ Å, as well as the space group $194\_P63/mmc$. Subsequently, we carried out the optimization of the following parameters: the exchange-correlation potential, the number of k-points, and the RKmax parameter, which determines the basis set's size.

3.1 Silicon

For Silicon, we employed the generalized gradient approximation (GGA) for the potential, along with the parametrization proposed by Perdew, Burke, and Ernzerhof (PBE). Our calculations included 2000 k-points and the RKmax parameter set to 9.0. With these previously optimized parameters, we conducted a volume optimization procedure, resulting in a revised lattice constant of $a = 5.4730$ Å as determined by the Birch-Murnaghan equation of state. Figure 4 illustrates Silicon's conventional cell, which is the elemental unit of the crystalline structure, while the graph in Figure 4 shows the volume of the structure at which the energy of the system reaches its minimum value.

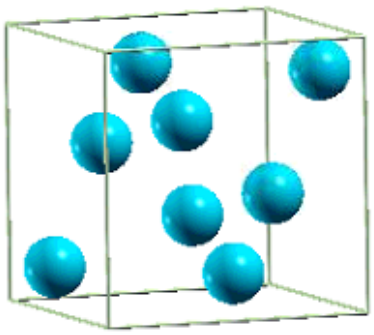

Figure 3: Conventional cell of Silicon

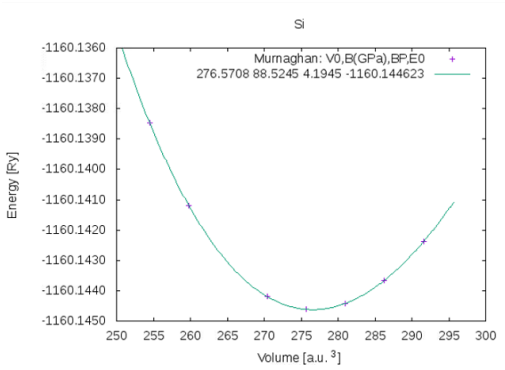

Figure 4: Volume optimization result.

Once the correct structure of the material of interest has been obtained, a wide range of properties can be studied. Our focus is on the level spacing distribution of the crystal's energy spectra. To calculate this distribution, we first require the material's band

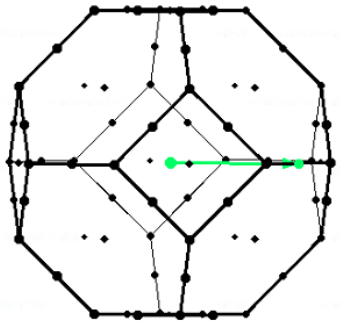

Figure 5: Primitive Brillouin zone of Si. The green line specifies the selected k-path from Γ to K.

structure. The initial step in computing the band structure is to determine the k-points in the Brillouin zone we want to analyze (Figure 5).

As previously stated, to find chaotic behavior in the energy level distribution, it is necessary to stay away from the symmetry points of the system. In a crystalline structure, this means staying away from the symmetry points of the Brillouin zone. For our purposes, we decided to restrict the analysis of the band structure between the Γ point at the center of the zone, and the point K at the boundary. Figure 6 shows Silicon's band structure, which was computed using 1000 k-points in the selected path. Upon a rapid examination of the band structure, it becomes evident that at the Γ point, the bands are closely packed. This outcome aligns with the expectations, considering our proximity to a symmetry point. As we proceed away from the Γ point, the separation between bands becomes noticeable. However, when the bands reach the K boundary, some of them converge again, while others remain separated. Therefore, when aiming to observe chaotic behavior in crystalline structures like Si, it is advisable to avoid the vicinity of symmetry points within the Brillouin zone.

Another important observation regarding the computed band structure is the presence of a limited number of widely spaced bands situated below the Fermi level, which defines the highest energy an electron can have when the system is at absolute zero temperature (Kittel & McEuen, 2018). In contrast, the bands maintain progressively closer proximity as we ascend above the Fermi level to higher energies. It is equally crucial to note the existence of gaps between certain bands where we would anticipate encountering more extensive distances between them. These variations in bandwidth could potentially impact the distribution of level spacing and should be considered when pursuing the identification of chaos.

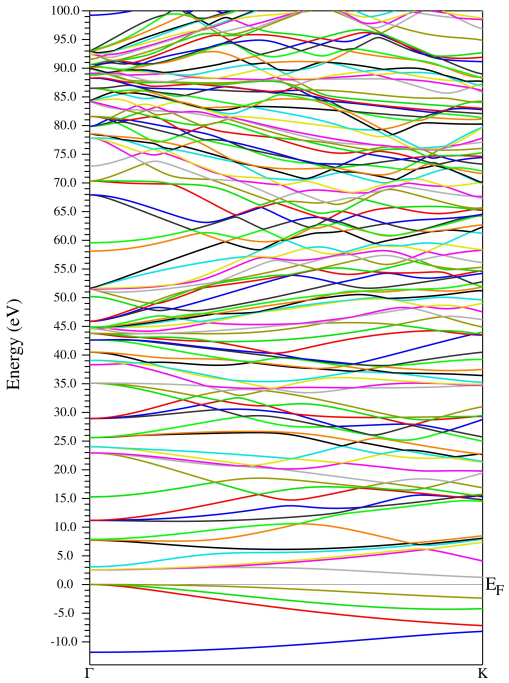

Figure 6: Si band structure in energies between -10.0 eV to 100.0 eV. The x-axis represents the k-points in the selected Brillouin zone path from Γ to boundary K.

In order to validate the accuracy of our calculations, we conducted an analysis of the band gap within the band structure. The band gap is defined as the separation between the minimum energy point of the first band above the Fermi level, referred to as the conduction band, and the maximum energy point of the valence band, which is the final band before E_F (Kittel & McEuen, 2018). For the computation of the band gap, we employed the modified Becke-Johnson potential, a computational resource available in the WIEN2K software package. Utilizing this approach, we obtained a band gap value of 1.19 eV. The discrepancy between this calculated value and the experimentally measured band gap (Camargo-Martínez & Baquero, 2013), which stands at 1.17 eV, is minimal, with a relative error of 1.7%.

3.2 Cerium

Similar to the approach used for Silicon, the band structure of Cerium was obtained through the application of the Generalized Gradient Approximation to derive the potential, using the PBE parametrization. These calculations were conducted employing 1000 k-points and setting the RKmax parameter to 9.0.

With the specified parameters in place, we proceeded with the optimization of lattice parameters. In the case of Cerium, we chose to focus on optimizing the c/a ratio

instead of the volume due to the chosen space group. This optimization process yielded the c/a ratio, represented in terms of one optimized lattice parameter c and one of the original lattice parameters a_{exp}. Specifically for Cerium, we identified the optimized lattice parameters as $a = 3.80342$ Å and $c = 5.95844$ Å. Figure 7 illustrates Cerium's conventional cell. As can be observed, Ce possesses a hexagonal structure, which is why a volume optimization equivalent to the one performed on Silicon cannot be employed here. Figure 8 illustrates the variation in the c/a ratio, showcasing the point at which energy attains its minimal value while preserving a constant volume.

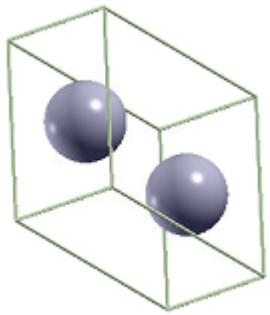

Figure 7: Conventional cell of Cerium.

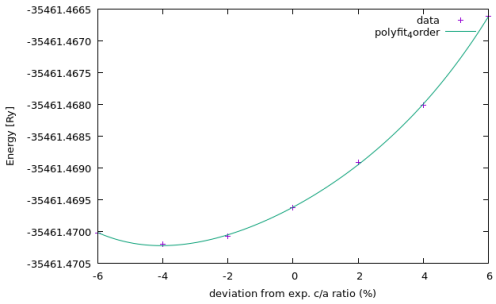

Figure 8: Volume optimization result. Selected k-path in the primitive Brillouin zone.

Subsequently, in Figure 9, we present the primitive Brillouin zone of Cerium (Ce). Our chosen k-path once again extends from the center point of the Brillouin zone, denoted as Γ, to the boundary point K.

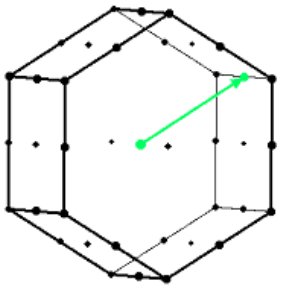

Figure 9: Primitive Brillouin zone of Ce. The green line specifies the selected k-path from Γ to K.

Utilizing 1000 k-points along this selected path, we obtained the band structure for Cerium. Figure 10 shows the band structure of Ce without Hubbard's correction and with a trial U= 6 eV respectively. Upon initial examination, the band distribution obtained through the calculation without the U parameter seems to have fewer bands than

the band structure where the parameter was implemented. In both cases, the bands exhibit a dense arrangement across the spectrum. However, significant distinctions become apparent when analyzing the bands around the Fermi level. This specific region is where the influence of the U parameter is expected to become evident due to the presence of electrons in the *d* and *f* orbitals.

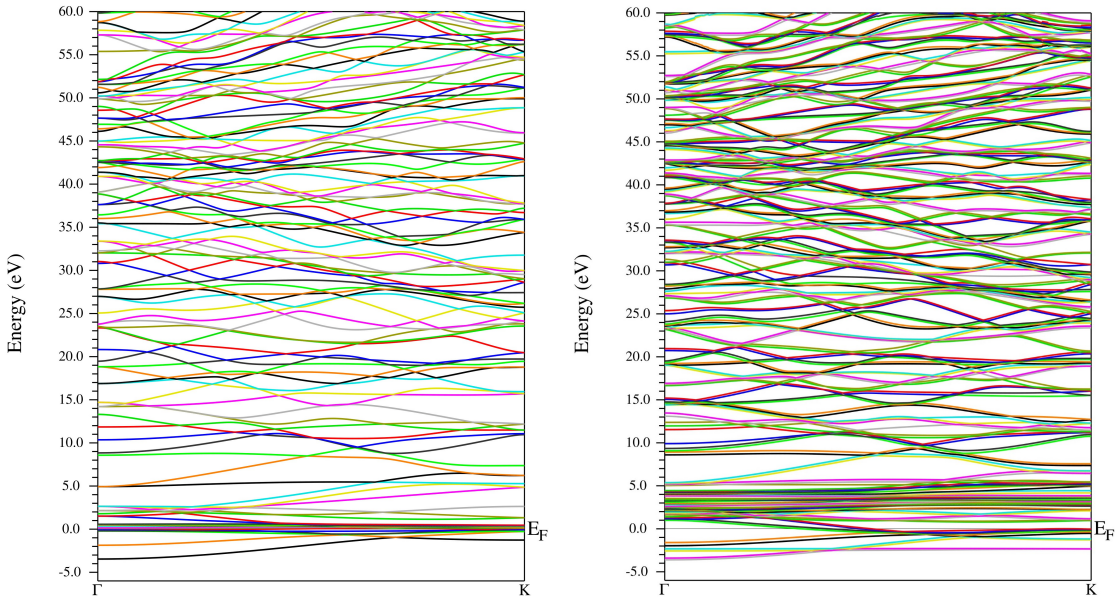

Figure 10: Cerium band structure from Γ to K. (a) No Hubbard correction. (b) Hubbard correction parameter set to U= 6 eV.

As illustrated in Figure 10b, where Hubbard's parameter was implemented, there is a notable shift in the region where bands are clustered together. In this figure, clustered bands go from above the Fermi level to approximately 5.0 eV. Conversely, in Figure 10a, this region seems to manifest at lower energies, extending from below E_F to roughly 3.0 eV. Furthermore, in the calculation where the Hubbard parameter was omitted, we clearly observe that the densely packed bands begin to separate around the K point. These notorious disparities between band structures can lead to significant variations in level spacing distributions. Such variations may facilitate the detection of quantum chaos induced by minor perturbations in the system.

Finally, it is also worth conducting an analysis of the Density of States (DOS) for the various Cerium calculations. The Density of States provides valuable information about the distribution of electrons within the crystal. It also allows us to discern how individual atomic orbitals contribute to the band structure and the influence of the Hubbard correction on it (Himmetoglu, Floris, De Gironcoli, & Cococcioni, 2014). Given our specific

research objective of investigating the impact of the Hubbard correction on the Cerium band structure, it is particularly important to examine both the total density of states for Ce and the contributions of the $4f$ and $5d$ electrons, since these orbitals are the ones the U parameter's primary affects.

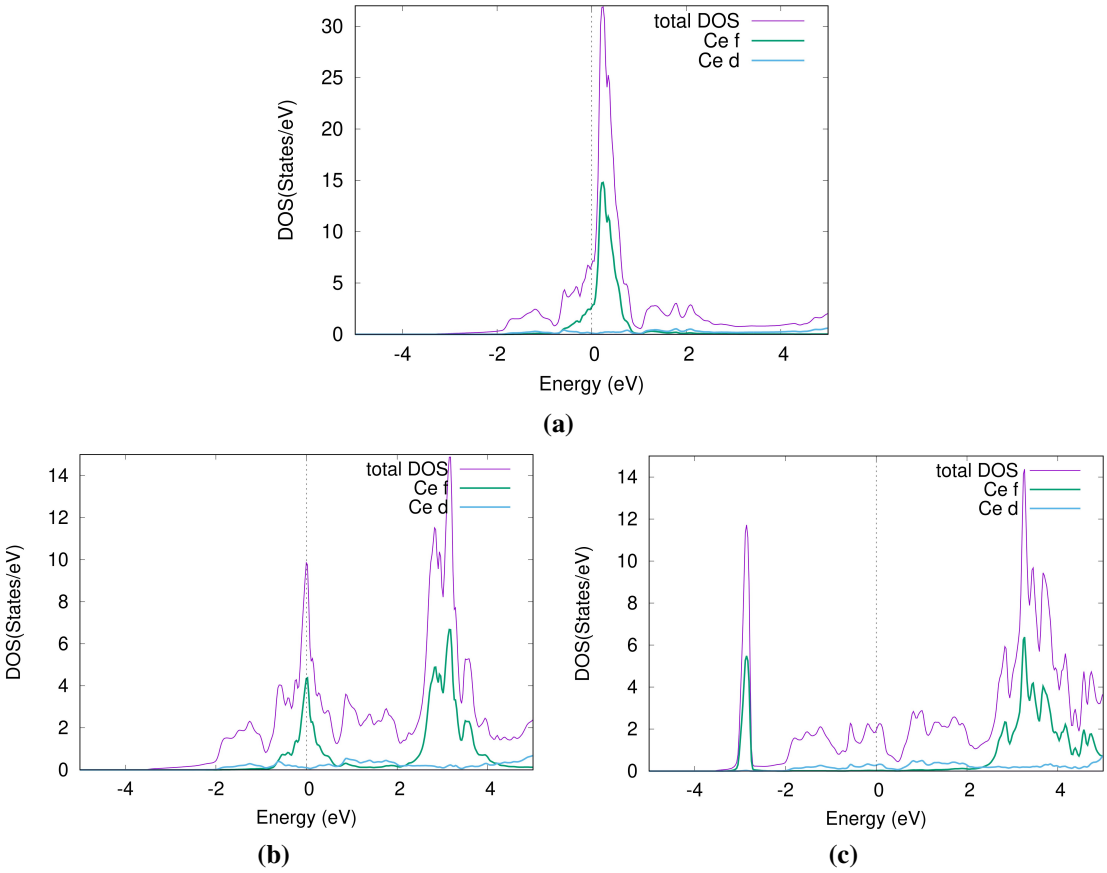

Figure 11: Density of States for Cerium with different values of U parameter. (a) No Hubbard correction. (b) U= 6 eV. (c) U= 7 eV.

Figure 11a presents the Density of States for the Cerium calculation in which the Hubbard correction was not applied. Notably, there is no band gap in Cerium, confirming its metallic nature in comparison with Silicon, which is categorized as a semiconductor with a well-established band gap. Furthermore, around 0.0 eV, the majority of the density contribution comes from the f orbital, while the contribution from the d orbital is minimal in this energy range. In terms of the band structure, this energy range corresponds to the location of the first energy bands immediately above the Fermi Level. Consequently, we deduce that a valuable approach to understanding the effect of the Hubbard correction on the $4f$ electrons is to study the first bands above 0.0 eV, as we anticipate that

these bands will undergo changes when electron correlation effects are considered. This approach is further supported by Figures 11b and 11c, which illustrate the Density of States of Ce when the Hubbard parameter was set to 6 eV and 7 eV, respectively. From these Figures, it is clear that the Hubbard correction modifies the energy regions where we will encounter influences from the f electrons. As a result, this behavior is likely to alter the band structure in the region above the Fermi level, making it a worthwhile subject for analysis.

3.3 Level Spacing distributions

The distribution derived from the spacing between neighboring eigenvalues represents one of the most frequently employed methodologies for describing the statistical properties of energy spectra (Reichl, 2004). In the context of crystalline materials, the level spacing is defined as the energy separation between two consecutive bands for a specific k-point. In order to obtain the complete level spacing distribution, it is necessary to traverse all the k-points along a specified path within the Brillouin zone and determine the energy differences between neighboring bands at each of these k-points. For numerical calculations of the distance between identical k-points in the i-th band and its neighbor, we utilize the following expression:

$$s_i = \frac{|\epsilon_i(k) - \epsilon_{i+1}(k)|}{\Delta} \tag{28}$$

Where Δ is the average over all the level spacing values in the region of the spectrum being analyzed (Mucciolo et al., 1994).

Silicon

We initiate our exploration of quantum chaos by examining the level spacing distribution of Silicon (Si), intending to replicate the findings of Mucciolo (Mucciolo et al., 1994) as reported in his paper. Mucciolo proposes that the manifestation of quantum chaotic behavior is feasible even in crystals with simple structures, such as Silicon. Figure 12 illustrates the level spacing distribution derived from the band structure of Silicon. The data set utilized for constructing this distribution was sourced from 85 bands situated above the Fermi level, each consisting of 1000 k-points. It is essential to note that our analysis primarily focuses on high-energy bands, as Mucciolo suggests that these bands are more likely to exhibit chaotic behavior.

From the initial level spacing distribution, one can see that a substantial number of values are situated near zero. This indicates that the selected bands are close to each

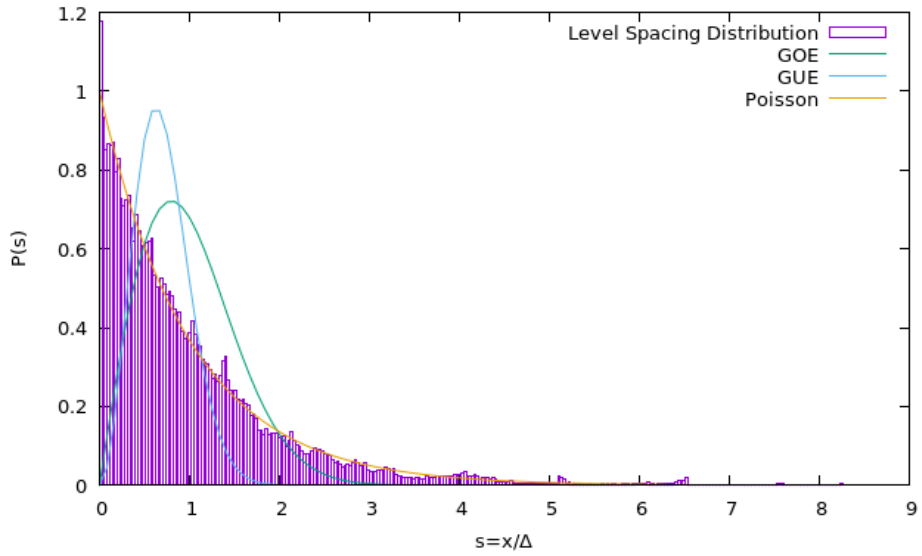

Figure 12: Si level spacing distribution from bands 5 to 90 and from k-point 1 to 1001.

other at multiple points, resulting in a distribution reminiscent of the Poisson distribution. This outcome aligns with expectations, as it was observed that near the Γ point, the bands exhibited significant degeneracy. To detect chaotic behavior, Mucciolo suggests avoiding the symmetry points within the Brillouin zone to prevent multiple values from clustering near zero.

Hence, we opted to restrict our analysis to the k-points located in the middle of the path under investigation. By meticulously examining the band structure, we identified the section presented in Figure 13a, comprising 85 k-points across 24 bands spanning between energies of 5.0 eV to almost 45.0 eV. Figure 13b illustrates the distribution derived from the selected bands. It is apparent that the level spacing distribution is in better agreement with the Gaussian Orthogonal Ensemble (GOE) prediction. This behavior is anticipated due to the reduction in level spacing values near zero achieved by utilizing k-points positioned away from symmetry points as Mucciolo recommends.

Furthermore, a pair of widely separated bands can be spotted in Figure 13a. These bands start close together at the Γ point with an energy of around 8.0 eV, then abruptly diverge to create a considerable gap at the middle of the selected k-path. The influence of gaps like the one mentioned is manifested in the level spacing distribution. Notably, around energy separations of 3.5 eV, the obtained distribution distinctly deviates from the GOE curve. Consequently, it is imperative to exercise caution around regions where the distance between bands appears significantly wider, as these structural gaps undeniably affect the distribution.

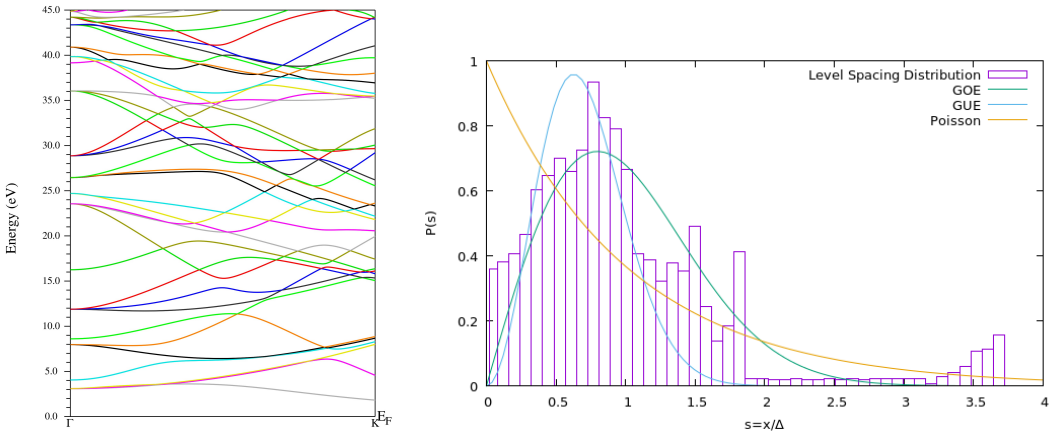

Figure 13: (a) Si band structure in the energy range from 5.0 eV to 45.0 eV, between the Γ and K point of the Brillouin zone. (b) Si level spacing distribution from bands 9 to 33 and from k-point 510 to 595.

Another collection of bands where chaotic behavior is apparent is provided in Figure 14. This set consists of 11 bands distributed in energies ranging from 25.0 eV to almost 40.0 eV. Figure 14a shows a close examination of the bands selected. It is clear that the selected bands are in close proximity to one another near the Γ point, aligning with expectations. As we traverse the k-point space, the bands progressively diverge, with many of them actively repelling each other as we approach the boundary at K within the Brillouin zone. This behavior is precisely what we seek, as it is within such regions that we can observe quantum chaos, as previously demonstrated.

The resultant distribution derived from the chosen bands is shown in Figure 14b. The examination of this specific band set is carried out employing 200 k-points positioned between the Γ point and the midsection of the k-space. This choice is made to evade the wide gap between the bands situated near the K points in the energy range from 30.0 eV to 35.0 eV. It is notable that, once again, the distribution closely aligns with the GOE prediction across the majority of its range.

The distributions acquired through the analysis of Si band structure show the feasibility of identifying chaotic behavior within simple crystalline structures, as Mucciolo proposed. A careful examination of the band structure enabled the identification of band sets whose distributions follow the predictions of random matrix theory. In both of the band collections examined minor deviations between the obtained distributions and the GOE curve were anticipated, as it is not possible to entirely eliminate the symmetries inherent to the system. It is finally important to remark that, even though the regions of the band structure where chaos is found are short in range, this is not something we should be concerned about since, according to Mucciolo, finding chaos in short ranges of

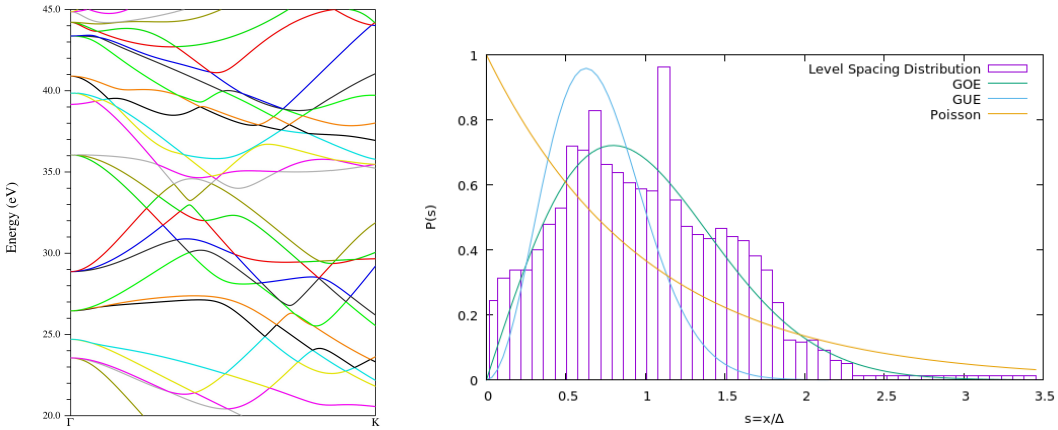

Figure 14: (a) Si band structure in the energy range from 20.0 eV to 45.0 eV, between the Γ and K point of the Brillouin zone. (b) Si level spacing distribution from bands 22 to 33 and from k-point 155 to 350.

the spectrum is expected due to the prevalence of symmetric features along the k-point space.

Cerium

Having demonstrated that specific segments of Silicon's band spectrum exhibit chaotic behavior in line with the expectations of random matrix theory, we are now keen to investigate other materials where evidence of quantum chaos might offer insights into their structure and properties. Among these materials, the study of the structure and band distribution of Cerium is particularly intriguing.

Cerium is classified as a rare-earth metal, possessing one electron in the $4f$ orbital and another in the $5d$ orbital. The positioning of valence electrons in rare-earth elements contributes to the stability of their optical transitions in the presence of electric fields, high temperatures, and other perturbations. This stability arises from the electrons in the fully occupied $5s$ and $5d$ orbitals, which create a shielding effect, protecting the valence electrons (Pomrenke, Klein, & Langer, 1993). Consequently, it is a logical choice to incorporate rare-earth metals like Cerium into semiconductors, as their valence electrons are less susceptible to the influences of the host material when doped. Furthermore, the potential applications of rare-earth-doped semiconductors enhance the significance and attractiveness of studying these systems.

Nevertheless, the presence of these outer electrons makes Cerium a complex system to describe using DFT due to the strong interactions between them. As mentioned earlier, when studying such systems, it is advantageous to employ Hubbard's U param-

eter, which takes into account the Coulomb and exchange interactions among the outer electrons. However, there is no universally accepted method for determining the precise value of the U parameter. Its optimal value appears to vary depending on the system under analysis and the specific property being investigated (Loschen, Carrasco, Neyman, & Illas, 2007). Thus, the Hubbard U parameter is often treated as an empirical or semi-empirical parameter, adjusted to align with the objectives of each study.

To gain insight into determining the most appropriate value for Hubbard's U parameter in describing Cerium, we compare level spacing distributions for six different calculations of the band structure. In one calculation, the Hubbard correction is omitted, while in the remaining five calculations, we vary the value of the Coulomb interaction term U in eq.(24) while keeping the exchange term J=0 constant.

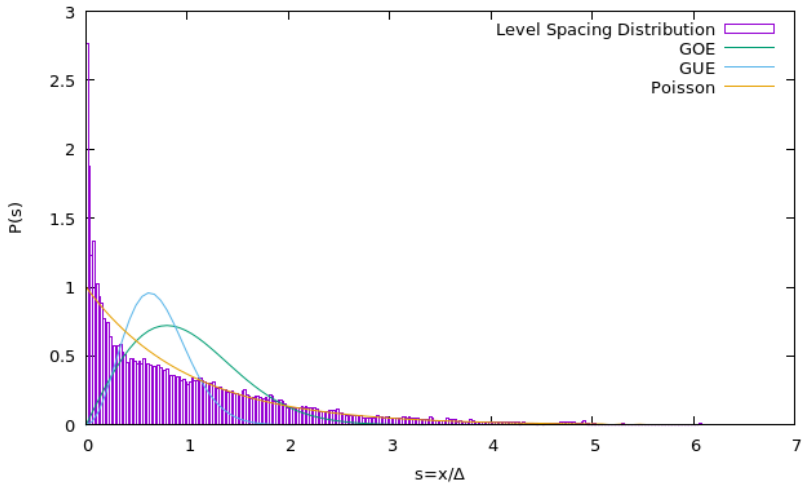

Figure 15: Ce level spacing distribution, calculated without U correction, from bands 15 to 100 and from k-point 1 to 1001.

Firstly, Figure 15 illustrates the level spacing distribution obtained from the Cerium calculation in which the U parameter was not included. The dataset used to construct this distribution comprises 85 bands above the Fermi level, each computed with 1000 k-points. We observe a good agreement with the Poisson curve, which is an expected behavior due to the degeneracy of bands near symmetry points.

The level spacing distributions for Cerium calculations where the Hubbard correction is employed, consisting of 165 bands and 1000 k-points, can be located in the Appendix. These distributions exhibit slight deviations from the Poisson curve but do not closely align with any Gaussian distribution. Furthermore, note that as the Hubbard correction parameter increases, the number of level spacing values near zero gradually decreases.

However, to investigate the influence of the Hubbard parameter on Cerium's band

structure, it is more suitable to narrow our analysis to the bands situated around the Fermi level. As we have already observed from the Density of States in Figure 11a, these bands are particularly influenced by the valence electrons and the strong correlations among them when the Hubbard correction is not considered, making them an interesting region to investigate differences in band structure calculations. Furthermore, it remains crucial to avoid the Γ point and the Brillouin zone boundary to minimize the number of level spacing values close to zero. As demonstrated in the previous analysis of Silicon, avoiding symmetry points enhances the probability of encountering chaotic behavior.

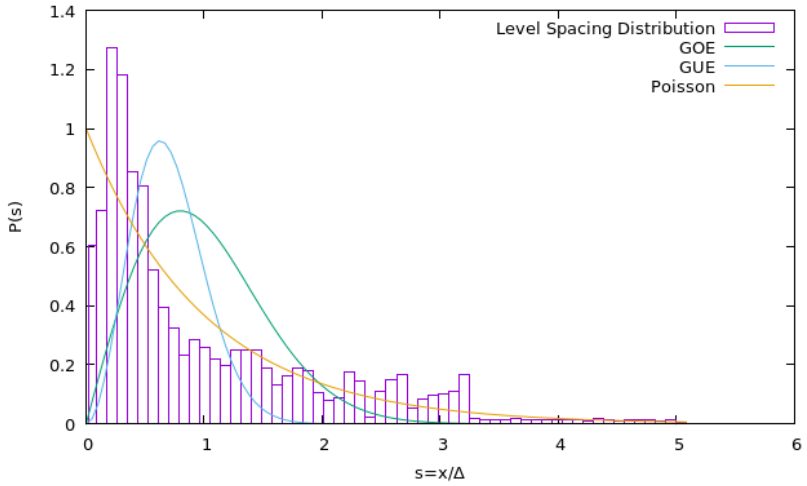

Figure 16: Ce level spacing distribution, calculated without U parameter, from bands 15 to 26 and from k-point 350 to 650.

Figure 16 displays once more the level spacing distribution obtained from the band structure computed without the U parameter. However, in this case, we considered only 11 bands starting from the conduction band and beyond. Additionally, the band spacing distribution was constructed using just 300 k-points situated in the middle of the selected path, far away from the symmetry points.

The most notable characteristic of this distribution is the sharp decline in level spacing values near zero, which is likely a consequence of avoiding the Γ and K points in the analysis. Nonetheless, it is still possible to observe some agreement with the Poisson curve rather than with the other distributions, indicating that chaotic behavior cannot be clearly identified in this level spacing distribution.

We will now examine the level spacing distributions derived from calculations employing Hubbard's correction. For each calculation, we implement a different value of the U parameter. Figures 17a to 17e illustrate the band spacing distributions in which the Coulomb interaction parameter was modified, varying from 4 eV to 8 eV, respectively,

meanwhile the J term, responsible for the exchange interaction, remains consistently at zero. These five distributions were constructed using the first 11 bands above the Fermi level and 300 k-points situated at the midpoint of the selected path in the Brillouin zone.

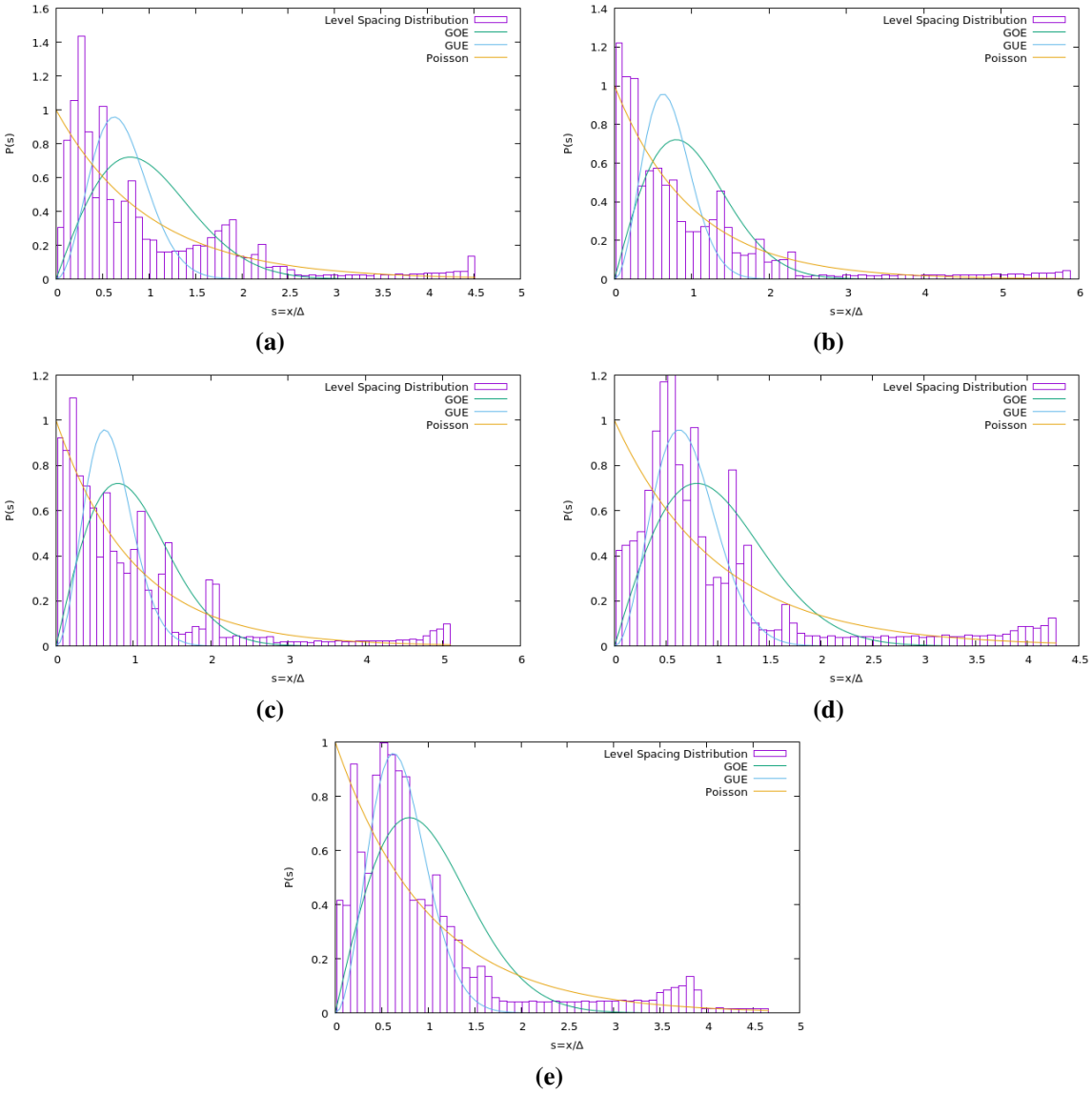

Figure 17: Level spacing distribution involving 11 bands and 300 k-points in Cerium for Hubbard corrections: (a) U=4 eV, (b) U=5 eV, (c) U=6 eV, (d) U=7 eV and (e) U=8 eV.

From the presented set of graphs, the most notable feature is that as the selected value for the Hubbard parameter increases, the distribution aligns better with the GUE curve. Figure 17a displays the level spacing histogram derived from the band structure where U was set to 4 eV. This distribution resembles the histogram obtained from the calculation

where the U approximation was omitted, with the exception that the discrepancies with the Poisson approximation are more pronounced. On the other hand, Figures 17b and 17c closely adhere to the Poisson curve, indicating the presence of multiple symmetric features in the Cerium band structure when these values for Hubbard's correction are applied. Thus, for the first three selected values of the U parameter, a precise diagnosis of quantum chaos is not achievable in the selected set of bands.

Figure 17d displays the level spacing distribution generated from the calculation where the Coulomb interaction parameter was set to 7 eV. Notice the sharp decrease in level spacing values near zero and the improved agreement with the GUE prediction. Finally, Figure 17e shows the distribution derived from the calculation that employed U=8 eV. We once again notice certain agreement with the GUE curve and the most notable deviation from the RMT predictions in this distribution is the slight increase in level spacing values close to zero.

As previously mentioned, obtaining the correct Hubbard parameter for each system through precise calculations is highly desirable. In 1991, Anisimov and Gunnarson (V. Anisimov & Gunnarsson, 1991) compared various results from different studies that aimed to calculate the precise value of U for Cerium using DFT. They concluded that values in the range of 6-7 eV were in excellent agreement with experimental data, and subsequently, other researchers (Harmon, Antropov, Liechtenstein, Solovyev, & Anisimov, 1995; Zhang et al., 2011) have tended to adopt Hubbard's parameter within this range when studying Cerium. From the level spacing distributions obtained, it is important to discuss the fact that, as we transition between the U values proposed by Anisimov and Gunnarson to correctly describe Cerium, the distribution shifts from a Poisson to a GUE curve. Furthermore, this good agreement with the GUE prediction continues for larger values than the ones recommended in Anisimov and Gunnarson's work.

This behavior has prompted us to question whether there exists a relationship between correctly choosing the Hubbard parameter for a certain system and the transition to chaos of the level spacing distribution when the correct parameter is employed. Furthermore, we wonder if this relationship holds for other rare-earth metals and strongly correlated systems.

3.4 Velocity distributions

Another relevant quantity we encounter when analyzing the band structure of crystals is the velocity of the electrons in each energy band. For a given band, the velocity is related to the change in energy that an electron experiences as it moves across the k-space. When considering a wave packet composed of multiple electron wavefunctions, the velocity of

the wave packet is referred to as the group velocity, defined as $v_g = \hbar^{-1} d\epsilon/dk$ (Kittel & McEuen, 2018). Numerically, to calculate the velocity of an electron moving within a specific band, the finite difference method is employed. Specifically, the central finite differences approximation is used, and it is given by:

$$\frac{d\epsilon(k)}{dk} = \frac{\epsilon(k + \Delta k) - \epsilon(k - \Delta k)}{2\Delta k} \tag{29}$$

Further information can be deduced from the group velocity. For instance, if we differentiate the group velocity with respect to time, we obtain:

$$\frac{dv_g}{dt} = \frac{1}{\hbar} \frac{d^2\epsilon}{dk^2} \frac{dk}{dt} \tag{30}$$

and knowing that we can represent an external force acting on an electron as $F = \hbar \frac{dk}{dt}$, we can write:

$$F = \left(\hbar^2 \frac{1}{d^2\epsilon/dk^2} \right) \frac{dv_g}{dt} \tag{31}$$

Finally, from Newton's second law, we identify the group velocity derivative as the acceleration and therefore the term in brackets as a mass term. We define the effective mass m as:

$$\frac{1}{m} = \frac{1}{\hbar^2} \frac{d^2\epsilon}{dk^2} \tag{32}$$

Where the second derivative of energy with respect to k represents the curvature of the energy band. The curvature is an additional property of the band structure that can provide valuable insights into the material under investigation. Further exploration of this property remains a subject for future research.

Silicon

We begin analyzing the velocity distribution of Silicon. Figure 18 presents the velocity distribution of the Silicon band structure. This distribution was constructed using 85 bands above the Fermi level, each containing 1000 k-points. It is important to note that the bands selected are the exact same bands used to construct the level spacing distribution in Figure 12. This choice was made to maintain continuity within the analysis. Upon examining the graph, we initially observe that the distribution reaches a maximum near $v/\Delta = 0$. Subsequently, we detect that the occurrence of specific velocity values progressively decreases as we move to higher velocities. This behavior suggests that Silicon velocities present a Gaussian-type distribution, indicating that the majority of the

selected bands do not demonstrate abrupt changes in their energy, which would lead to high velocities. Instead, their energy changes gradually as they traverse the k-space.

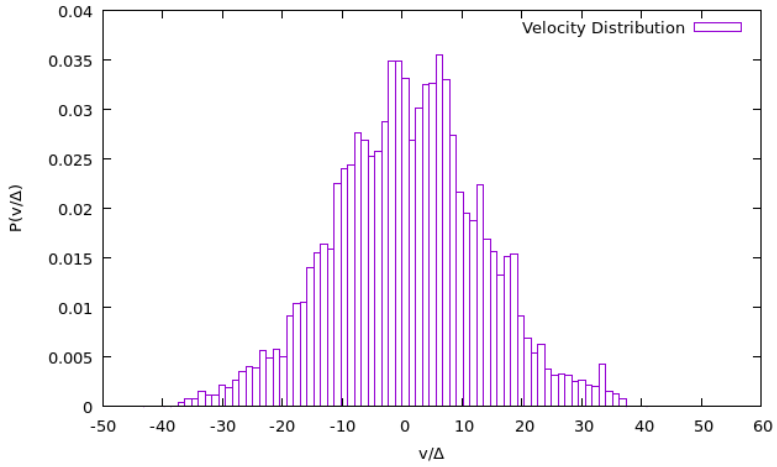

Figure 18: Silicon velocity distribution constructed using 85 bands, each with 1000 k-points. The constant Δ is the average over all the velocity values.

Cerium

The velocity distributions for different calculations of the Cerium band structure are now presented. Figure 39 displays the velocity distribution of 65 high-energy bands, each containing 1000 k-points. These bands correspond to the Ce calculation where Hubbard's correction was not included. When comparing this distribution to the one for Silicon in Figure 18, certain similarities come to light. Notably, both distributions prominently exhibit a prominent peak for velocity values close to zero. However, this time, we observe a sharper decrease in the number of velocity values as we move away from zero, in comparison with the gradual decrease observed in the case of Silicon. This behavior indicates that there are minimal abrupt changes in the energy of the bands throughout the k-space.

Moreover, it is worth highlighting that the peak in the velocity distribution of Cerium reaches substantially higher values on the y-axis when compared to the peak in the Silicon distribution. However, as we move away from $v/\Delta = 0$, the Cerium distribution begins to closely resemble the behavior observed in the Silicon distribution. This intriguing observation suggests that the key distinction between the velocity distributions of Silicon and Cerium lies in the higher number of bands in Cerium with slopes close to zero.

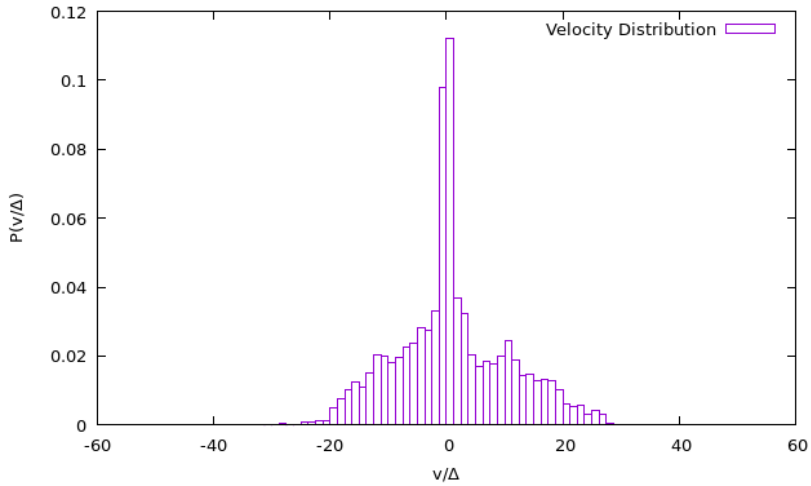

Figure 19: Cerium velocity distribution constructed using 65 bands, each with 1000 k-points.

Further information can be deduced by comparing the previous distribution with the velocity distributions obtained from calculations in which the Hubbard correction was applied. These distributions are available in the Appendix. However, we will concentrate our analysis of the Ce structure on a reduced set of bands near the Fermi level since it has been discussed that this is one of the regions where the correction effect of the U parameter can be better observed. Figure 20a presents the energy range where the first 11 bands above E_F are located. Notice that most of the bands selected between 0.0 eV and 1.0 eV do not show significant changes in their energy as they extend through the k-space. Only the last band abruptly decreases its energy as it moves away from the Γ point.

Following the band structure, Figure 20b presents the velocity distribution constructed using the aforementioned 11 bands. This analysis focuses exclusively on 300 k-points located between the Γ point and the Brillouin zone boundary at K. This particular k-point selection is made to exclude regions where bands exhibit degeneracy, as these regions can significantly influence the distribution as has been already discussed. We observe in this graph a significant increase in the concentration of velocity values around zero compared with the previous distributions, an expected behavior since most of the bands being analyzed are almost in a completely horizontal position, but there is also an evident decline in values at higher velocities. An essential characteristic of this graph, aside from the prominent peak around zero, is that the majority of non-zero values are positive. This implies that, within the selected region, most changes in bands lead to higher energy levels.

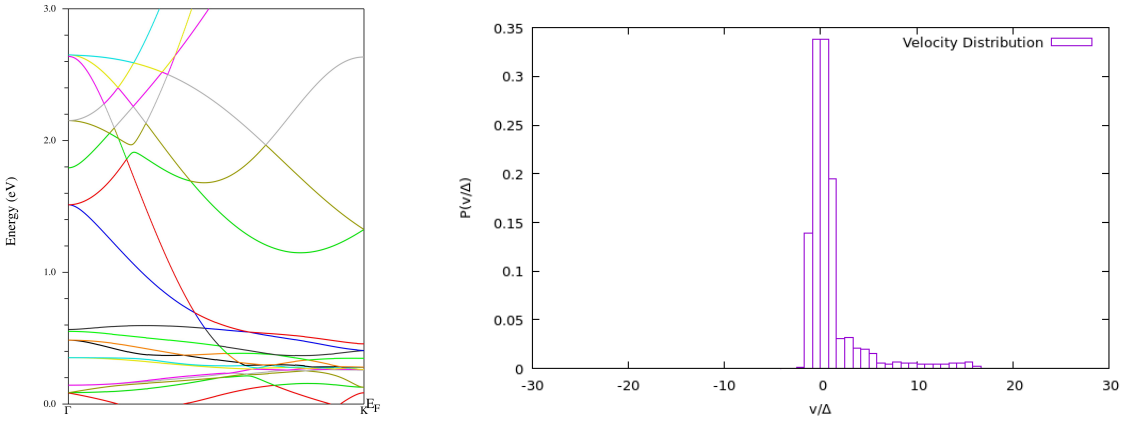

(a) **(b)**

Figure 20: Cerium band structure and velocity distribution without Hubbrad's correction (a) Ce band structure between 0.0 eV and 3.0 eV (b) Ce level spacing distribution from bands 15 to 26 and from k-point 350 to 650

The subsequent figures illustrate the band structures and velocity distributions for calculations incorporating the Hubbard correction. Once again, our analysis is focused on the initial 11 bands situated above the Fermi level, utilizing a set of 300 k-points positioned at the center of the k-space. Figures 21a, 22a, and 23a show Cerium band structure, where Hubbard's correction was applied through the parameter values U= 4 eV, U= 6 eV, and U= 8 eV, respectively. It is apparent that as the value of the parameter U increases, the bands immediately above the Fermi level gradually move farther apart. Additionally, the separation between bands is accompanied by a noticeable increase in the steepness of their slopes, a behavior that is likely to impact the velocity distribution.

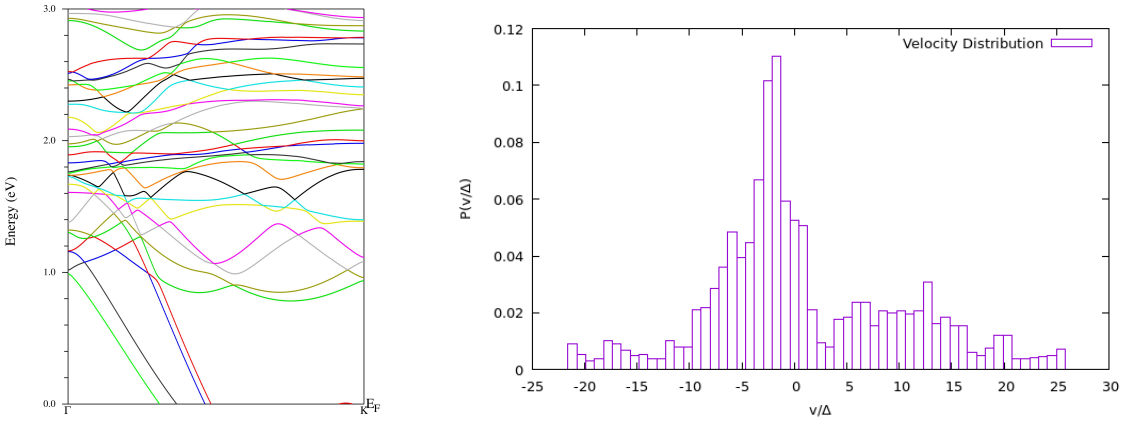

(a) **(b)**

Figure 21: Cerium band structure and velocity distribution with U= 4 eV. (a) Ce band structure between 0.0 eV and 3.0 eV. (b) Ce level spacing distribution from bands 27 to 38 and from k-point 350 to 650.

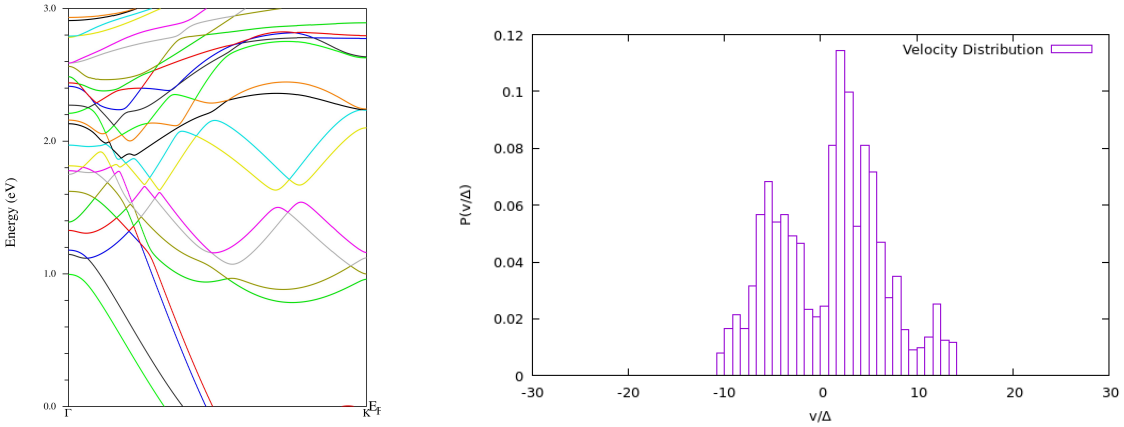

(a) **(b)**

Figure 22: Cerium band structure and velocity distribution with U= 6 eV. (a) Ce band structure between 0.0 eV and 3.0 eV. (b) Ce level spacing distribution from bands 27 to 38 and from k-point 350 to 650.

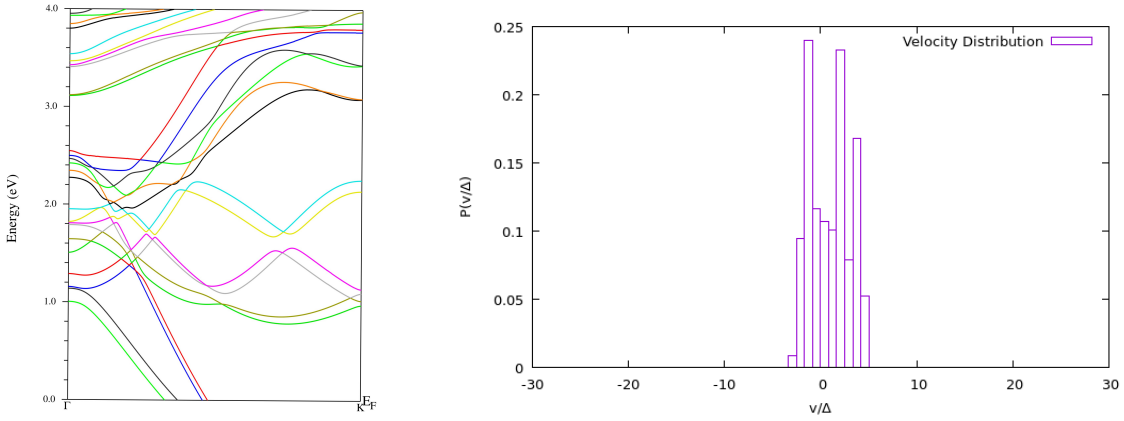

(a) **(b)**

Figure 23: Cerium band structure and velocity distribution with U= 8 eV. (a) Ce band structure between 0.0 eV and 3.0 eV. (b) Ce level spacing distribution from bands 27 to 38 and from k-point 350 to 650.

In the figures adjacent to the band structures, we present the velocity distributions obtained using the various U values employed. Overall, the distributions reach almost the same maximum value in the y-axis except for Figure 23b, where the maximum reached value is way above the other distributions. Figure 21b was derived from the calculation with U set to 4 eV. Notice the reduction in the number of velocities near zero and the shift of the distribution peak towards negative values. This pattern indicates that most of the changes in the bands result in lower velocities.

Similarly, the distribution in Figure 22b, obtained using the U= 6 eV calculation, displays a more pronounced decline in the number of velocity values around zero. However, this distribution exhibits a more symmetrical appearance, with a distinct peak at positive velocity values. This distribution suggests that most of the bands experienced fluctuations in their energy as they traversed the k-space and that there were almost no regions where bands maintained constant energy.

Finally, the distribution obtained from the U= 8 eV band structure, as presented in Figure 23b, once again demonstrates a significant decrease in velocity values around zero. However, it is worth noting that this distribution displays two peaks, one for negative velocities and the other for positive velocities. The distribution maximums reach much higher values on the y-axis compared to the two previous distributions. This phenomenon can be attributed to the repulsive interactions between bands, which result in the elevation of certain bands to higher energy levels while simultaneously lowering the energy of the bottom bands. This leads to steeper slopes and, consequently, explains the substantial increase in velocity values.

4 Conclusions

In this study, we examine the statistical properties of two different crystalline structures. Specifically, we focused on the analysis of the level spacing and velocity distributions within the band structures of Silicon and Cerium, with the aim of identifying chaotic behavior in line with the predictions of Random Matrix Theory.

In the case of Silicon, we successfully identified regions within its band structure where the level spacing distribution closely adheres to the Gaussian Orthogonal Ensemble (GOE) curve. This discovery allowed us to identify chaotic behavior within the Silicon structure, thereby replicating Mucciolo's findings and supporting his hypothesis that quantum chaos can manifest when we focus on regions in the Brillouin zone far away from the symmetry boundaries, even in apparently simple crystalline systems. It's important to note that the chaotic behavior we encountered was observed in different energy ranges compared to those in which Mucciolo initially identified quantum chaos. This disparity was expected due to the methodology employed in this thesis, which involved Density Functional Theory (DFT) with the generalized-gradient approximation (GGA) for the exchange-correlation functional. In contrast, Mucciolo utilized a total-energy pseudopotential approximation to model the electronic structure of Silicon. However, our findings show that even when distinct methods are employed, chaotic behavior is likely to manifest in specific regions of the Silicon band structure.

Shifting our focus to Cerium, we conducted an in-depth analysis of its band structure, concentrating on the first 11 bands situated above the Fermi Level. This specific region was selected after a meticulous examination of the Density of States, driven by the aim of studying the alterations in the band structure due to the contributions of the d and f orbitals when applying the Hubbard correction needed to correctly describe a strongly correlated system.

From this analysis, we arrived at interesting observations. First, we observed that without the Hubbard correction, the level spacing distribution from the bands around the Fermi level does not exhibit quantum chaos. Nevertheless, for U= 7 eV and U= 8 eV, the level spacing distribution of Cerium exhibited a closer agreement with the Gaussian Unitary Ensemble (GUE) curve, allowing us to identify chaotic behavior in this system. Additionally, we noted a transition from a Poisson distribution to a chaotic one between U= 6 eV and U= 7 eV, a commonly used range of values for describing Cerium accurately. Such a connection could imply that Random Matrix Theory can be a valuable tool when attempting to determine the precise value of the Hubbard parameter needed to accurately describe a strongly correlated system. Another question that arises is related to the accuracy of the Cerium structure obtained and whether it is worthwhile

to employ other methods apart from Density Functional Theory (DFT) to validate our findings. It is anticipated that alternative methods could yield similar results to those presented in this thesis but in different energy ranges, similar to our observations with Silicon. The exploration of these possibilities remains a subject for future research.

Furthermore, the wide variation in distributions observed for a specific system when altering a single parameter emphasizes the substantial impact of the Hubbard correction. Consequently, it is imperative to seek improved methods for determining the best approximation to the correct value of the U parameter needed to describe certain structures, depending on the method or approximation being used. We leave this subject for future investigation.

The analysis of velocity distributions for both Silicon and Cerium revealed interesting patterns. In the case of Silicon, which involved 85 bands, each with 1000 k-points, the velocity distribution closely aligned with a Gaussian curve. Likewise, the velocity distribution for Cerium without the Hubbard correction, within a similar energy range, exhibited Gaussian-like behavior for most velocity values, except in the vicinity of zero, where there was a significant increase in values. This behavior was also found in the velocity distributions of Cerium calculation where the Hubbard parameter was implemented. These distributions revealed that, in the majority of the Cerium spectrum, for both calculations with and without the Hubbard correction, most bands maintained relatively horizontal orientations or flat behavior, with minimal variations in their slopes. Nevertheless, for 11 bands around the Fermi Level and for different Hubbard correction parameter values, we observed a sharp decline in velocity values near zero. This decline can be attributed to the increasing repulsion between bands observed in the band structure around the Fermi Level as the U parameter rises.

These observations emphasize the sensitivity of the velocity distribution to subtle changes in the band structure and raise intriguing questions about the connection between velocity values and chaotic behavior. It prompts us to explore whether this statistical property can serve as a diagnostic tool for quantum chaos.

Lastly, we introduced the concept of curvature, a property closely linked to velocity, which shows potential for further examination. The exploration of this property, as well as the study of other statistical tools commonly employed in Random Matrix Theory to diagnose quantum chaos, such as the Δ_3 statistics, along with the investigation of the band structure in other regions of the Brillouin zone, remains open for future research.

5 Appendix

In this appendix, we provide supplementary figures designed to complement our primary research and findings. These additional figures serve as a tool to conduct a more in-depth analysis of the band structures of Silicon and Cerium. Specifically, the appendix includes supplementary information about level spacing and velocity distributions for various Cerium calculations.

5.1 Band structure

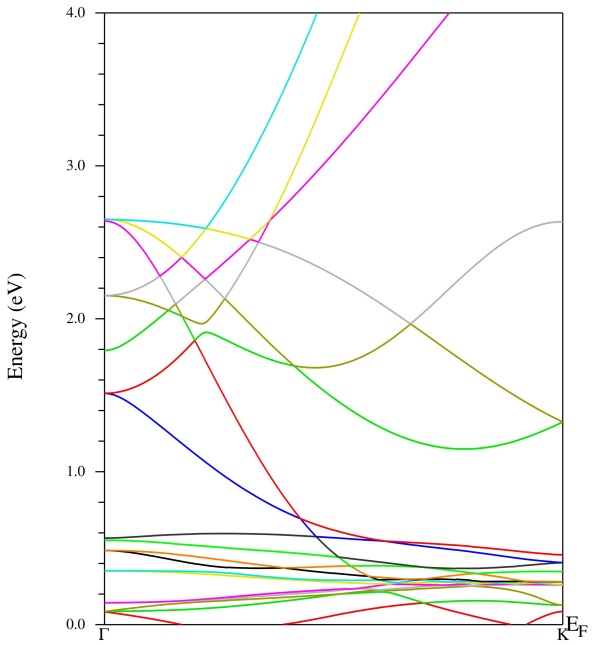

Figure 24: Band structure of Cerium without Hubbard's correction, between 0.0 eV and 4.0 eV. The energy range selected contains the first 11 bands above the Fermi Level.

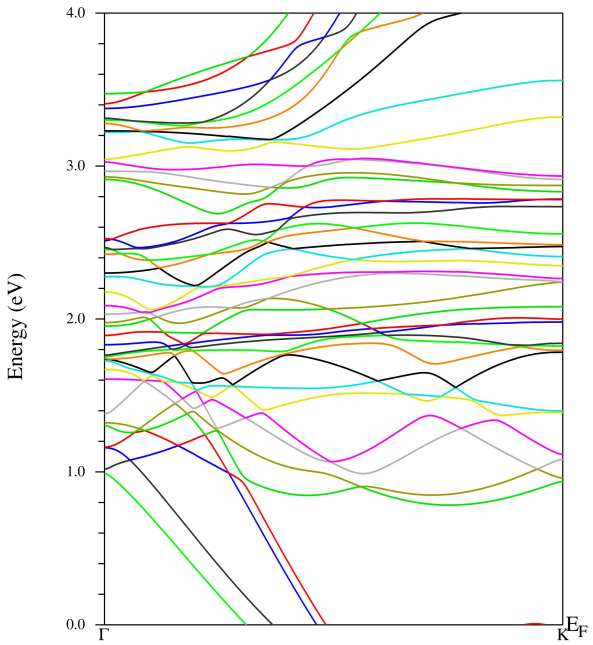

Figure 25: Band structure of Cerium with U= 4 eV, between 0.0 eV and 4.0 eV. The energy range selected contains the first 11 bands above the Fermi Level.

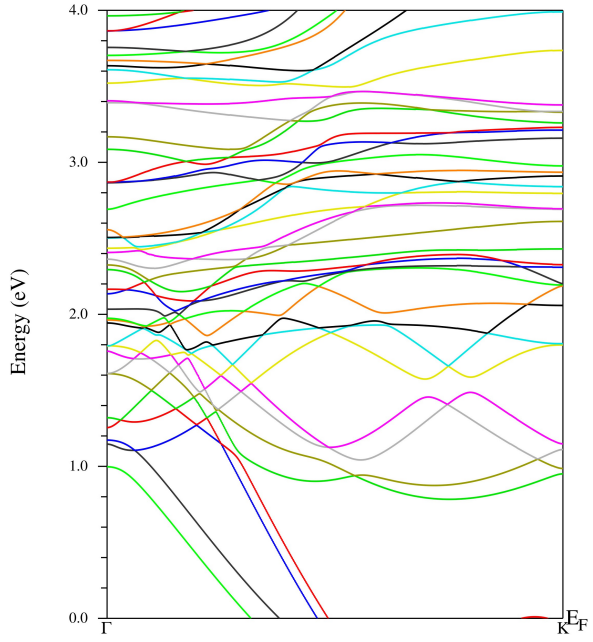

Figure 26: Band structure of Cerium with U= 5 eV, between 0.0 eV and 4.0 eV. The energy range selected contains the first 11 bands above the Fermi Level.

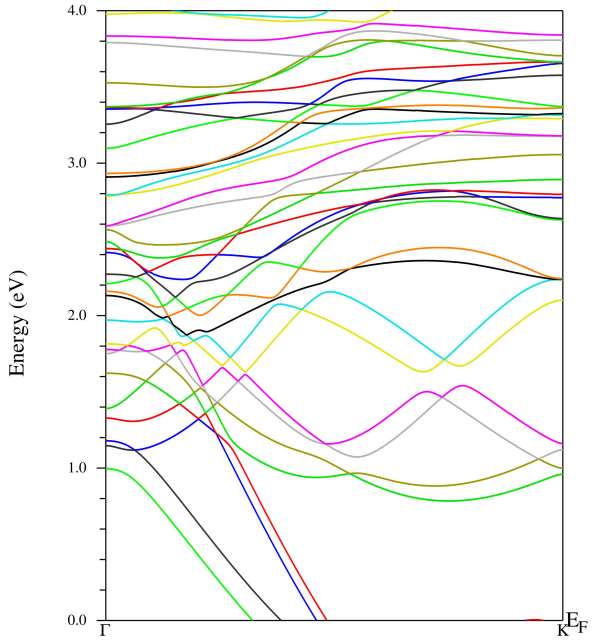

Figure 27: Band structure of Cerium with U= 6 eV, between 0.0 eV and 4.0 eV. The energy range selected contains the first 11 bands above the Fermi Level.

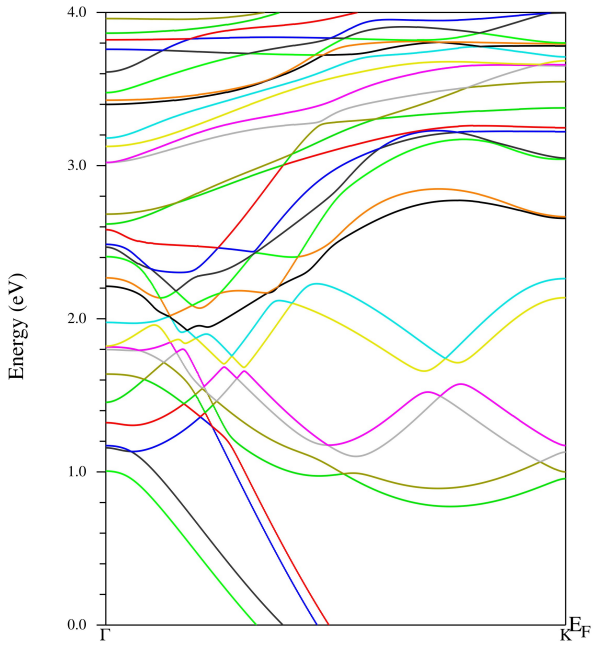

Figure 28: Band structure of Cerium with U= 7 eV, between 0.0 eV and 4.0 eV. The energy range selected contains the first 11 bands above the Fermi Level.

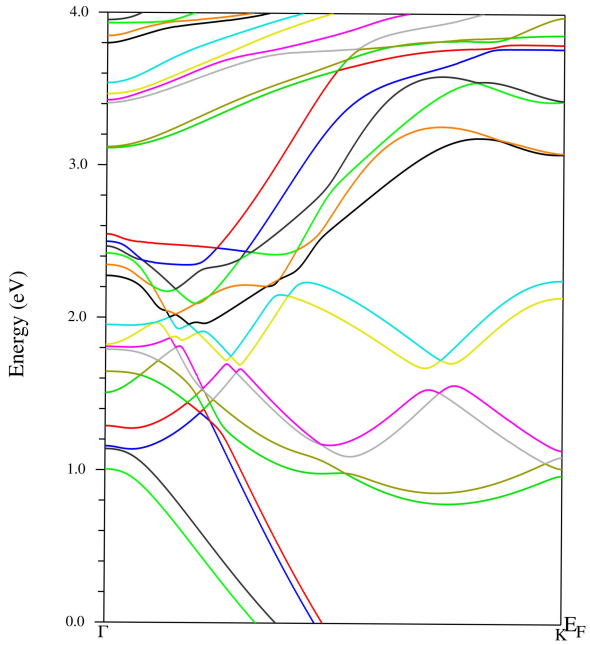

Figure 29: Band structure of Cerium with U= 8 eV, between 0.0 eV and 4.0 eV. The energy range selected contains the first 11 bands above the Fermi Level.

5.2 Level Spacing distributions

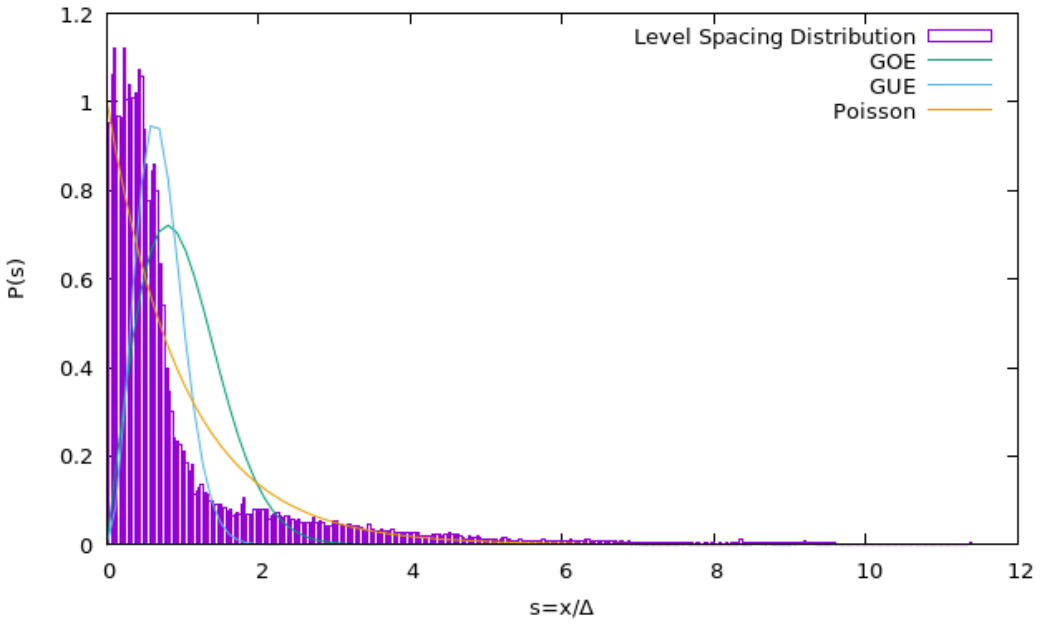

Figure 30: Cerium level spacing distribution constructed using 165 bands, each with 1000 k-points and U set to 4 eV.

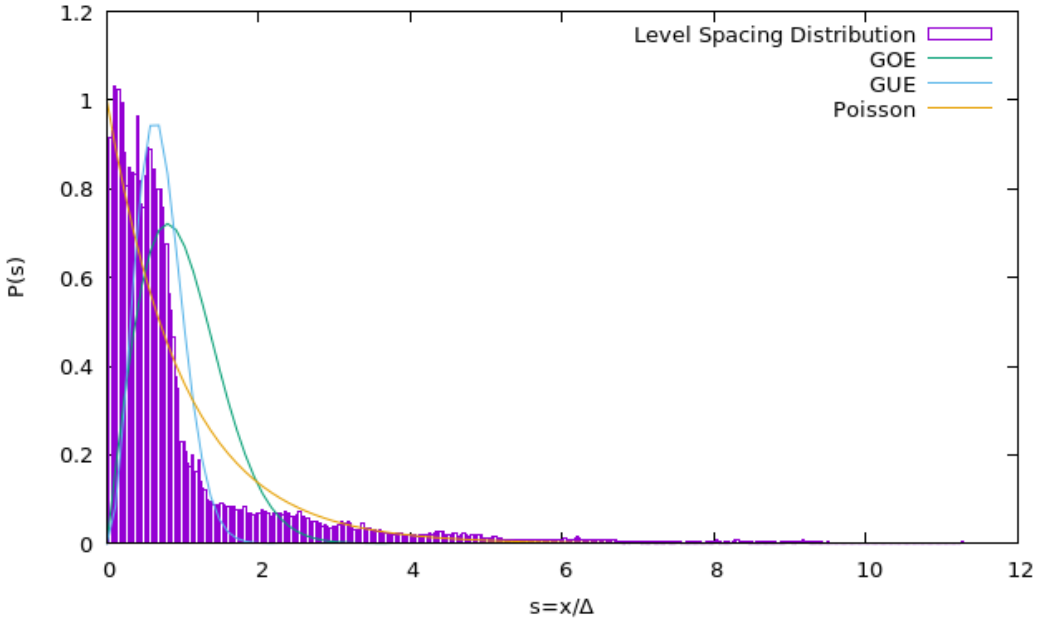

Figure 31: Cerium level spacing distribution constructed using 165 bands, each with 1000 k-points and U set to 5 eV.

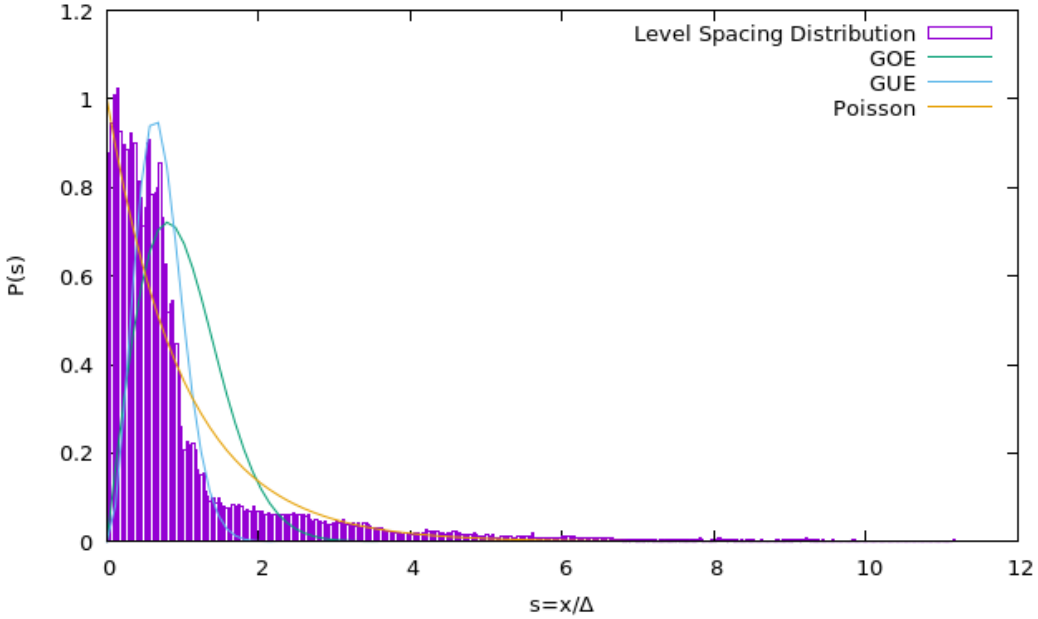

Figure 32: Cerium level spacing distribution constructed using 165 bands, each with 1000 k-points and U set to 6 eV.

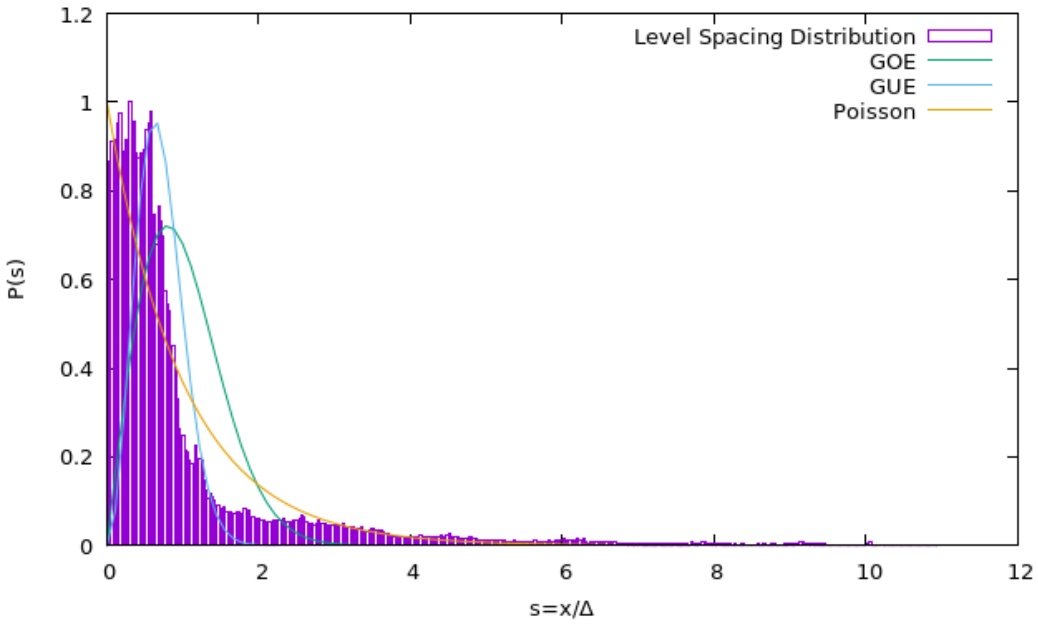

Figure 33: Cerium level spacing distribution constructed using 165 bands, each with 1000 k-points and U set to 7 eV.

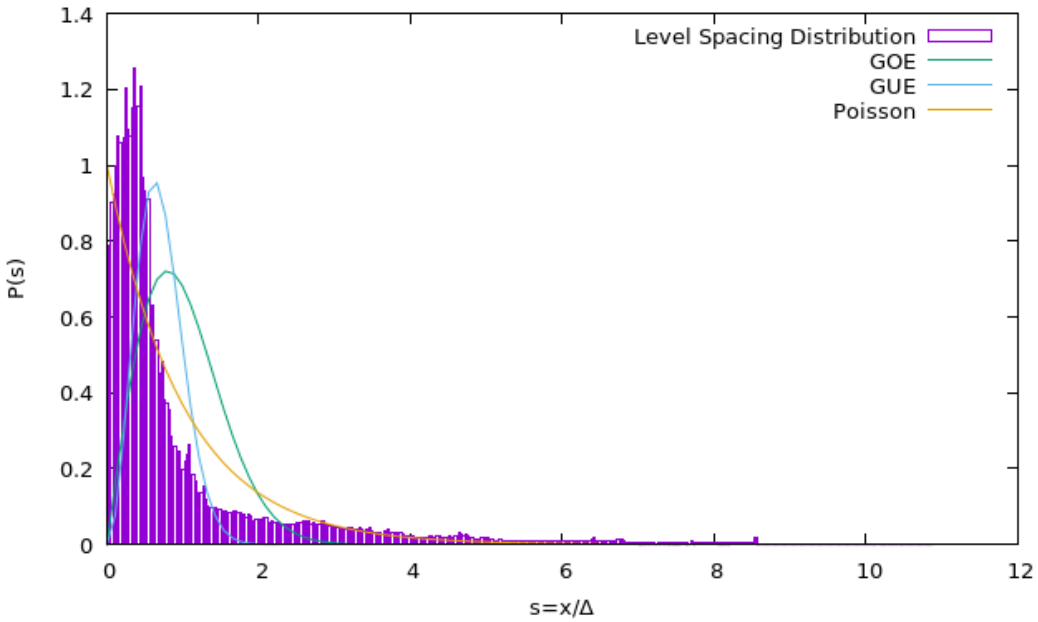

Figure 34: Cerium level spacing distribution constructed using 165 bands, each with 1000 k-points and U set to 8 eV.

5.3 Velocity distributions

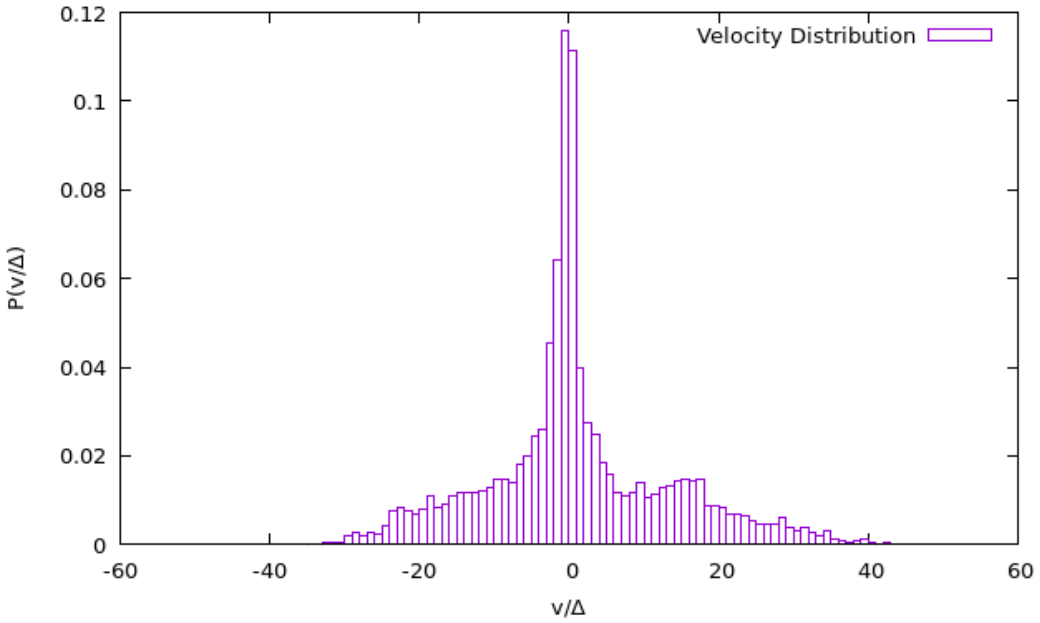

Figure 35: Cerium velocity distribution constructed using 113 bands, each with 1000 k-points and U set to 4 eV.

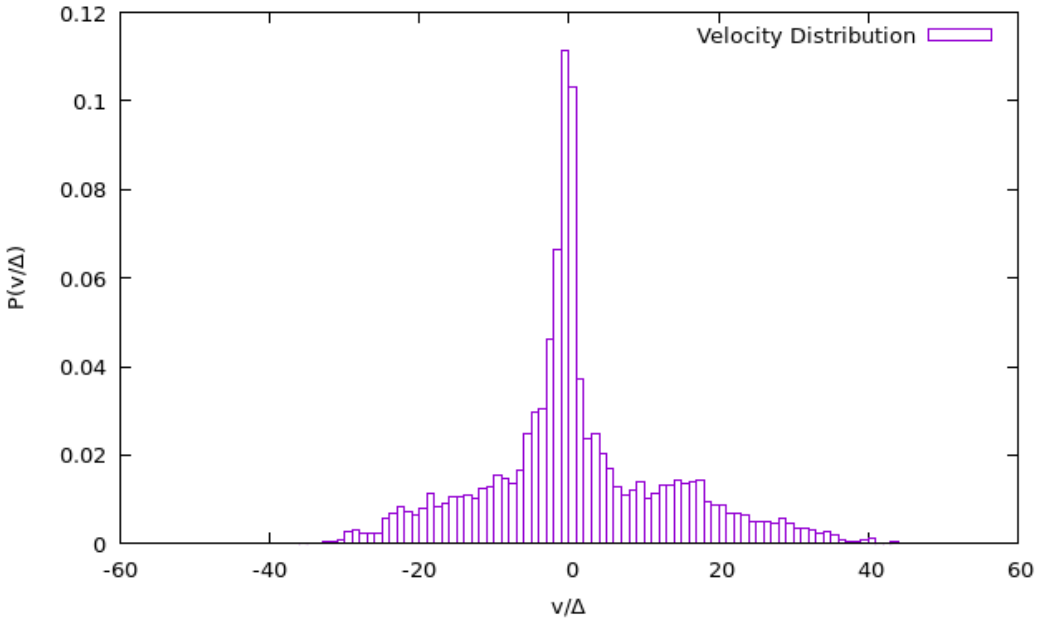

Figure 36: Cerium velocity distribution constructed using 113 bands, each with 1000 k-points and U set to 5 eV.

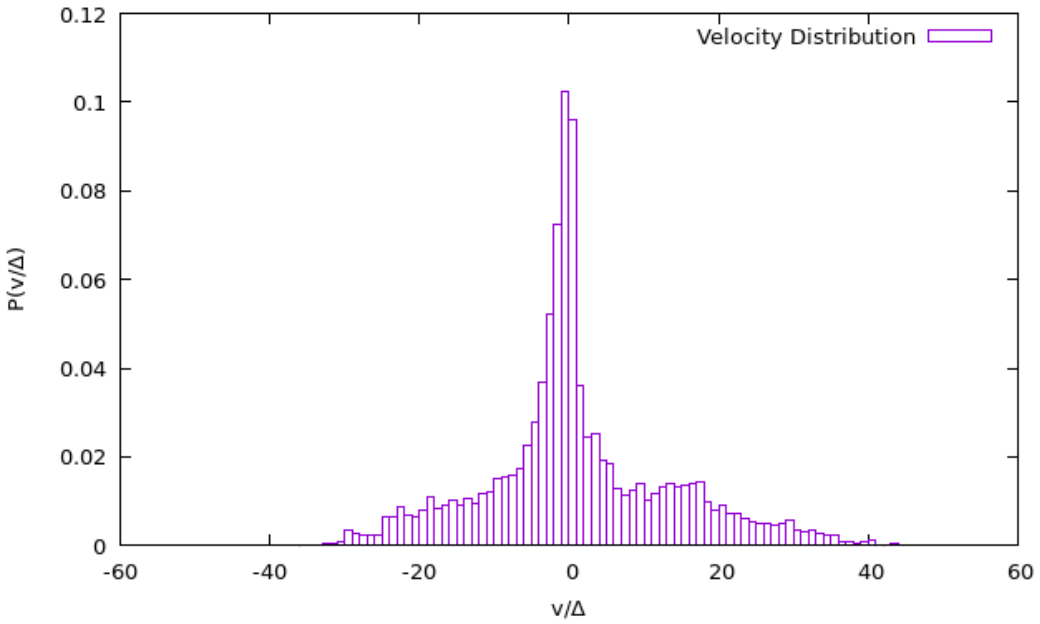

Figure 37: Cerium velocity distribution constructed using 113 bands, each with 1000 k-points and U set to 6 eV.

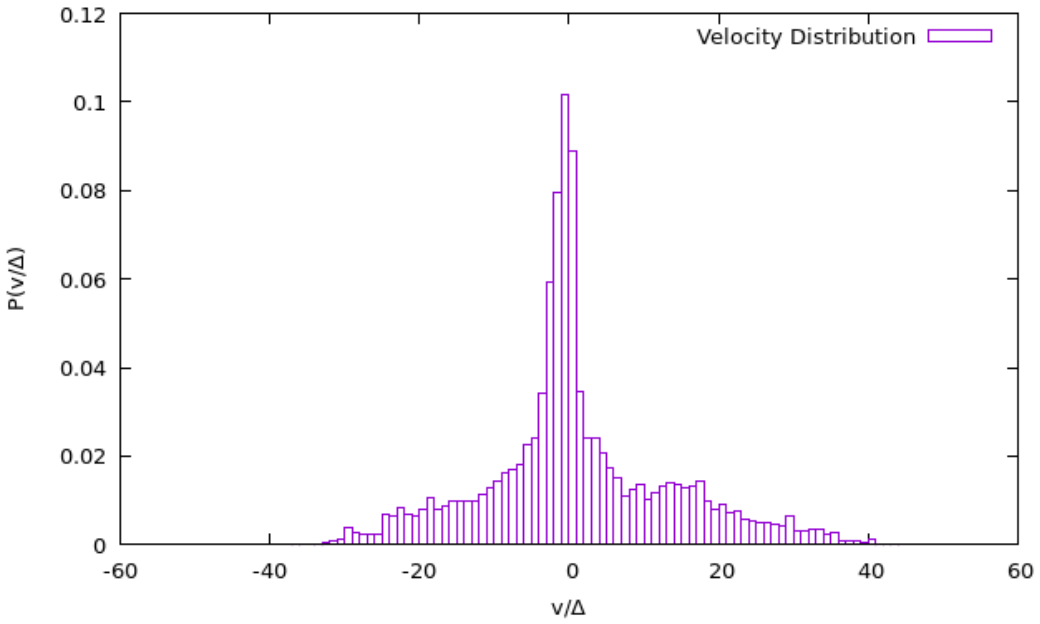

Figure 38: Cerium velocity distribution constructed using 113 bands, each with 1000 k-points and U set to 7 eV.

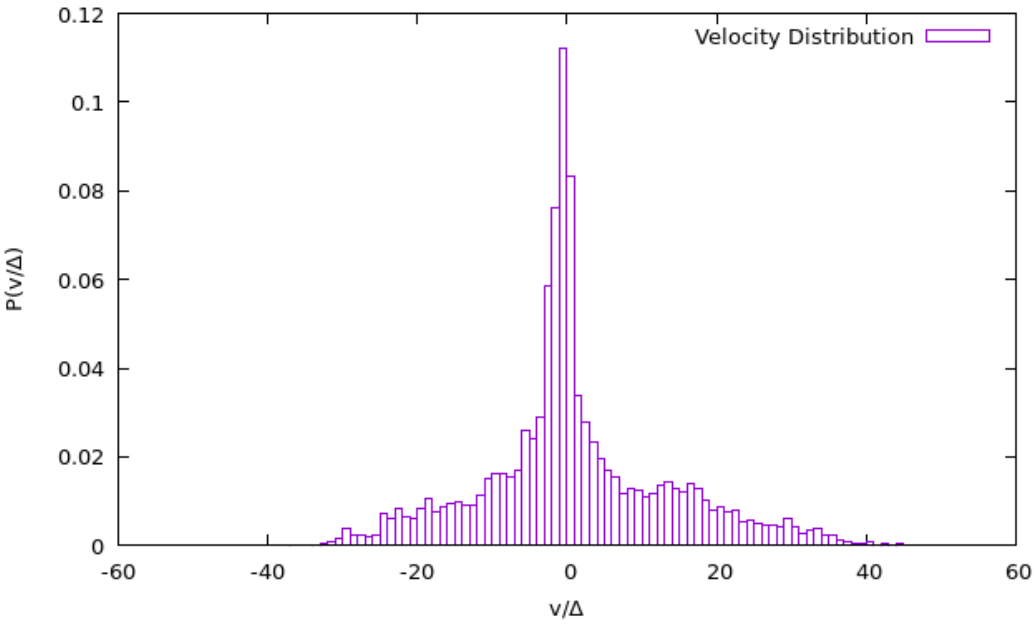

Figure 39: Cerium velocity distribution constructed using 113 bands, each with 1000 k-points and U set to 8 eV.

References

Anisimov, V., & Gunnarsson, O. (1991). Density-functional calculation of effective coulomb interactions in metals. *Physical Review B*, *43*(10), 7570.

Anisimov, V. I., Aryasetiawan, F., & Lichtenstein, A. (1997). First-principles calculations of the electronic structure and spectra of strongly correlated systems: the lda+ u method. *Journal of Physics: Condensed Matter*, *9*(4), 767.

Bennett, L. J., & Jones, G. (2014). The influence of the hubbard u parameter in simulating the catalytic behaviour of cerium oxide. *Physical Chemistry Chemical Physics*, *16*(39), 21032–21038.

Berry, M. (1989). Quantum chaology, not quantum chaos. *Physica Scripta*, *40*(3), 335.

Berry, M. V. (2001). Chaos and the semiclassical limit of quantum mechanics (is the moon there when somebody looks?). *Quantum Mechanics: Scientific perspectives on divine action*, *41*, 56.

Blaha, P., Schwarz, K., Madsen, G. K., Kvasnicka, D., Luitz, J., et al. (2001). wien2k. *An augmented plane wave+ local orbitals program for calculating crystal properties*, *60*(1).

Camargo-Martínez, J., & Baquero, R. (2013). The band gap problem: the accuracy of the wien2k code confronted. *Revista mexicana de física*, *59*(5), 453–459.

Chevalley, C. (1947). Theory of lie groups i. *Princeton, NJ*.

Dudarev, S., Castell, M., Botton, G., Savrasov, S., Muggelberg, C., Briggs, G., ... Goddard, D. (2000). Understanding stm images and eels spectra of oxides with strongly correlated electrons: a comparison of nickel and uranium oxides. *Micron*, *31*(4), 363–372.

Dyson, F. J. (1962). Statistical theory of the energy levels of complex systems. i. *Journal of Mathematical Physics*, *3*(1), 140–156.

Escalante, J. M., & Skipetrov, S. E. (2018). Level spacing statistics for light in two-dimensional disordered photonic crystals. *Scientific Reports*, *8*(1), 11569.

Gutzwiller, M. C. (2013). *Chaos in classical and quantum mechanics* (Vol. 1). Springer Science & Business Media.

Harmon, B., Antropov, V., Liechtenstein, A., Solovyev, I., & Anisimov, V.

(1995). Calculation of magneto-optical properties for 4f systems: Lsda+ hubbard u results. *Journal of Physics and Chemistry of Solids*, *56*(11), 1521–1524.

Himmetoglu, B., Floris, A., De Gironcoli, S., & Cococcioni, M. (2014). Hubbard-corrected dft energy functionals: The lda+ u description of correlated systems. *International Journal of Quantum Chemistry*, *114*(1), 14–49.

Hohenberg, P., & Kohn, W. (1964). Inhomogeneous electron gas. *Physical review*, *136*(3B), B864.

Kittel, C., & McEuen, P. (2018). *Introduction to solid state physics*. John Wiley & Sons.

Kohn, W., & Sham, L. J. (1965). Self-consistent equations including exchange and correlation effects. *Physical review*, *140*(4A), A1133.

Krane, K. S. (2019). *Modern physics*. John Wiley & Sons.

Loschen, C., Carrasco, J., Neyman, K. M., & Illas, F. (2007). First-principles lda+ u and gga+ u study of cerium oxides: Dependence on the effective u parameter. *Physical Review B*, *75*(3), 035115.

Luna-Acosta, G., Na, K., Reichl, L., & Krokhin, A. (1996). Band structure and quantum poincaré sections of a classically chaotic quantum rippled channel. *Physical Review E*, *53*(4), 3271.

Martin, R. M. (2020). *Electronic structure: basic theory and practical methods*. Cambridge university press.

McDonald, S. W., & Kaufman, A. N. (1979). Spectrum and eigenfunctions for a hamiltonian with stochastic trajectories. *Physical Review Letters*, *42*(18), 1189.

Mehta, M. (1967). Random matrices and the statistical theory of energy levels, acad. *Press, New York*.

Mucciolo, E., Capaz, R., Altshuler, B., & Joannopoulos, J. (1994). Manifestation of quantum chaos in electronic band structures. *Physical Review B*, *50*(12), 8245.

Perdew, J. P., Burke, K., & Ernzerhof, M. (1996). Generalized gradient approximation made simple. *Physical review letters*, *77*(18), 3865.

Pomrenke, G. S., Klein, P. B., & Langer, D. W. (1993). *Rare earth doped semiconductors* (Vol. 301). The Society.

Reichl, L. E. (2004). *Transition to chaos*. Springer.

Rosenzweig, N., & Porter, C. E. (1960). " repulsion of energy levels" in complex atomic spectra. *Physical Review*, *120*(5), 1698.

Schafer, T., Daelman, N., & Lopez, N. (2021). Cerium oxides without u: The role of many-electron correlation. *The Journal of Physical Chemistry Letters*, *12*(27), 6277–6283.

Sholl, D. S., & Steckel, J. A. (2022). *Density functional theory: a practical introduction*. John Wiley & Sons.

Strogatz, S. H. (2018). *Nonlinear dynamics and chaos with student solutions manual: With applications to physics, biology, chemistry, and engineering*. CRC press.

Szabo, A., & Ostlund, N. S. (2012). *Modern quantum chemistry: introduction to advanced electronic structure theory*. Courier Corporation.

Taylor, J. R., & Taylor, J. R. (2005). *Classical mechanics* (Vol. 1). Springer.

Wigner, E. P. (1967). Random matrices in physics. *SIAM review*, *9*(1), 1–23.

Zhang, Y. G., Zhang, G. B., & Xu Wang, Y. (2011). First-principles study of the electronic structure and optical properties of ce-doped zno. *Journal of Applied Physics*, *109*(6).